Characterization of Synchronizer Performance for a Clutchless Transmission

by

Amado Antonini

Submitted to the
Department of Mechanical Engineering
in Partial Fulfillment of the Requirements for the Degree of

Bachelor of Science in Mechanical Engineering

at the

Massachusetts Institute of Technology

June 2016

Signature of Author: Signature redacted
Department of Mechanical Engineering
May 6, 2016

Certified by: Signature redacted
Amos G. Winter
Assistant Professor
Thesis Supervisor

Accepted by: Signature redacted
Anette Hosoi
Professor of Mechanical Engineering
Undergraduate Officer

Characterization of Synchronizer Performance for a Clutchless Transmission

by

Amado Antonini

Submitted to the Department of Mechanical Engineering
on May 6, 2016 in Partial Fulfillment of the
Requirements for the Degree of

Bachelor of Science in Mechanical Engineering

ABSTRACT

Synchronizers are a ubiquitous component of almost every type of transmission in modern vehicles. They are mechanical devices whose function is to ensure that components rotating at different rates can be harmonized smoothly and without eroding their surfaces. They are responsible for both the durability of the transmission and the comfort of the passengers.

This work analyzes the capabilities and limitations of synchronizers to be used in a novel transmission. It is a contribution to a larger project whose goal is to develop a hybrid, clutchless transmission for a performance vehicle that will improve efficiency by eliminating the friction and mechanical losses inherent in a traditional clutch.

An overview of the synchronization process is presented followed by a simplified mathematical model of the common baulk-ring synchronizer. The model is experimentally validated in order to make predictions of the device's performance on the new transmission. Several simulated scenarios are then developed that provide information that is critical for designing synchronizers for the clutchless transmission. Matlab code was developed for these simulations and is provided at the end for replication of the results.

Considering the demanding environment under which the synchronizers are expected to operate in the clutchless transmission, the possible failure modes of the synchronizer components are investigated. Finite element analysis (FEA) is used to predict the maximum loads on the synchronizer ring before the material yields. An energy analysis is also performed to ensure that the energy dissipation rate of the friction surfaces is adequate.

Thesis Supervisor: Amos G. Winter, V
Title: Assistant Professor

ACKNOWLEDGEMENTS

This thesis work would not have been possible without the input of the people who helped me and supported me along the way. I would like to thank Professor Amos Winter for taking me into his lab to work on this project, which has been an incredible learning experience, and for his advice throughout the project. Many thanks to Dan Dorsch for providing me with great mentorship from the very beginning of this research. To Mark Belanger for assisting me in setting up the experiments and providing the necessary tools at the Edgerton Center, thank you for your time and expert advice. To Professor Pedro Reis who was also my professor in 2.002, thank you for your advice on material analysis. Thank you to Pierce Hayward for your help and technical advice in measuring material properties. Thank you to Professor Barbara Hughey from the 2.671 lab for providing the sensors used in the experiment.

I would like to give special thanks my mom, my dad, my grandma, my brothers, and my girlfriend for their incredible love and support not only during this thesis but also during my entire time at MIT. None of this would have been possible without you and you are my number one source of motivation. Lastly, a big thanks to all my friends at or outside MIT who have always supported me and in one way or another helped shape the person I am.

Table of Contents

List of Figures

List of Tables

Nomenclature

A_{car}	Frontal area of vehicle [m^2]
b_c	Half length of the cone generatrix [m]
ΔE_C	Change in energy of the car [J]
$E_{D,C}$	Energy dissipated in the car due to drag [J]
$E_{D,E}$	Energy dissipated in the engine due to drag [J]
E_{dis}	Energy dissipated by synchronizer [J]
ΔE_E	Change in energy of the car [J]
$\Delta E_{k,C}$	Change in kinetic energy of the car [J]
$\Delta E_{k,E}$	Change in kinetic energy of the engine [J]
$E_{S,C}$	Energy transferred from synchronizer to car [J]
$E_{S,E}$	Energy transferred from engine to synchronizer [J]
F_f	Fork force on the sleeve [m]
C_{rr}	Rolling resistance coefficient of tires [kg/Mg]
C_x	Air drag coefficient of vehicle [-]
D_{spdl}	Rotational drag coefficient of lathe [$kg \cdot m^2/s$]
g	Gravitational acceleration [m/s^2]
J_E	Engine inertia [$kg \cdot m^2$]
J_g	Engine inertia reflected on the gear [$kg \cdot m^2$]
J_h	Car inertia reflected on the output (hub) side of the synchronizer [$kg \cdot m^2$]
J_{spdl}	Spindle inertia [$kg \cdot m^2$]
m_{car}	Mass of the car [kg]
N_c	Number of cones [-]
R_c	Mean radius of the cone [m]
r_{ET}	Gear ratio from engine to transmission output [-]
r_{FD}	Final drive ratio between transmission output and wheels [-]
R_s	Mean radius of sleeve at point of contact with fork [m]
R_w	Wheels' radius [m]
t_f	Synchronization time [s]
v_{car}	Car speed [m/s]
α_c	Cone angle measured from the shaft axis [rad]
β_s	Flank angle of sleeve splines measured from sleeve travel direction [rad]
μ_c	Coefficient of friction between cones [-]

μ_f	Coefficient of friction between fork and sleeve [-]
μ_s	Coefficient of friction between teeth flanks [-]
ω	Engine angular velocity [*rad/s*]
ω_0	Initial engine angular velocity [*rad/s*]
ω_g	Angular velocity of the gear [*rad/s*]
ω_h	Angular velocity of the hub and output shaft [*rad/s*]
ω_{spdl}	Angular velocity of the spindle [*rad/s*]
$\tau_{C,spdl}$	Coulombic drag torque of the spindle [$N \cdot m$]
$\tau_{D,g}$	Drag torque of the engine reflected on the gear [$N \cdot m$]
$\tau_{D,h}$	Drag torque of the car reflected on the hub [$N \cdot m$]
τ_f	Fork torque [$N \cdot m$]
τ_I	Index torque [$N \cdot m$]
τ_{in}	Torque input for lathe parameter determination experiment [$N \cdot m$]
τ_s	Synchronization torque [$N \cdot m$]

1 INTRODUCTION

1.1 Motivation

The motivation behind this thesis project is to aide in the development of a clutchless hybrid transmission. This development is being conducted at the MIT GEAR lab in collaboration with a car manufacturer and the objective is to design a clutchless hybrid transmission for a performance sports car. This thesis focuses on characterizing the behavior of the synchronizers in the transmission so that the design of the latter can proceed taking into account the capabilities and limitations of the former. As in any vehicle transmission, in the proposed clutchless transmission synchronizers play the important role of bringing gears up (or down) to speed when shifting. But specifically in a clutchless transmission, without the clutch that normally isolates the internal combustion engine (ICE) from the transmission (and therefore from the synchronizers), the synchronizers must also synchronize the ICE to the relative speed of the wheels and the car given a certain gear. The inertia and drag of the ICE is very large compared to the combined inertia and drag of the transmission components that a synchronizer normally synchronizes. Those are the input shaft, the idler gears, the transmission-side clutch disk, and the layshaft [1]. It is therefore necessary to characterize the synchronizer's capabilities and limitations in this new configuration in order to ensure their proper function in the clutchless transmission.

1.1.1 Design of a Clutchless Transmission for a Performance Car

The clutchless transmission project is motivated by the opportunity to improve the efficiency of current transmissions by eliminating inertial, frictional, and mechanical losses. Additionally, removing the clutch can reduce the size and weight of the transmission. Specifically, the idea is to eliminate the friction clutch and instead utilize an electric motor to engage and disengage gears by speed and torque matching, which will be controlled by the car's embedded computer, the Electronic Control Unit (ECU) [2]. In current transmissions, gear shifting is achieved with the help of synchronizers that use friction to slow down the faster-spinning gear and speed up the slower-spinning gear until their speeds match and they can be mated. But because of the high inertia of the ICE, this is done simultaneously as the clutch separates the engine power from the transmission. In automatic manual transmissions (AMT) the clutch is controlled electronically [3] and in manual transmissions it is controlled manually.

The proposed clutchless hybrid transmission will eliminate the friction clutch. When a shift of gears is required, the ECU will bring the required gear up to the correct speed, adjust the speed of the ICE for engagement, and fill in torque towards the wheels while they are disconnected from the ICE, all by the means of one (or two) electric motor(s). The removal of the clutch simplifies the mechanics of the transmission and eliminates the energy loss due to friction and pumping of hydraulic fluid within the clutch. Moreover, the ability to apply torque on the wheels during shifting eliminates the gap in acceleration associated with traditional vehicles during a gearshift. These alterations have the potential to advance powertrain performance in hybrid vehicles [2].

Figure 1-1 shows a schematic of the dual electric motor design. In this design, one electric motor is used for starting the vehicle from stop (forward and reverse), filling in torque to the output shaft during shifting (hereinafter referred to as torque-fill), and for regenerative braking. The other electric motor is used for starting the ICE, for speed-matching gears during shifting, and as a generator for recharging the battery. Both motors can be used as an additional power source when high torque is demanded during regular driving [2].

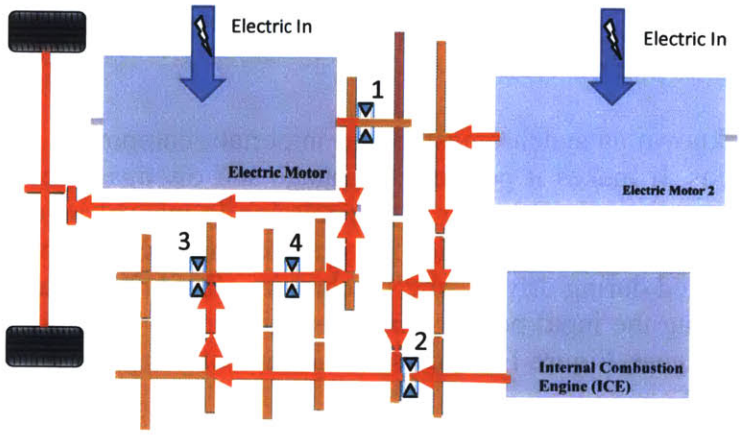

Figure 1-1: Schematic of clutchless transmission design (from [2])
The schematic shows the dual electric motor design of the clutchless transmission. The electric motor on the top left is used for launching, torque-fill, and regenerative braking. The one on the top right is used for starting the ICE, for speed-matching gears during shifting, and for recharging the battery. The red arrows represent the flow of power during regular driving both electric motors been used as an additional source of power during normal driving.

The synchronizer units are numbered 1 through 4 in Figure 1-1. In the specific driving situation depicted, with all three power sources engaged, synchronizers 1, 2, and 3 are engaged; they interlock their adjacent gear to the shaft on which they would otherwise free-spin.

1.1.2 Synchronizers in the Clutchless Transmission

The benefits achieved by removing the friction clutch and replacing it with an electric motor come at the cost of changing the synchronizer's role. In a traditional transmission the synchronizers are used to synchronize the rotational speed of engine-side components of the transmission (excluding the engine) which have relatively small inertia to the output shaft side. However in the clutchless transmission they will be needed to finish the synchronization between the ICE, with its large inertia, and the target gear. This synchronization will be started and almost finished by the ECU using either an electric motor to apply torque to the un-synchronized part of the gear train (now including the ICE), or by regulating the speed of the ICE directly through the fuel intake [2]. So the role of the synchronizers changes from synchronizing relatively small inertias with high speed differences in the order of $1000rpm$ to synchronizing relatively large inertias with small speed differences perhaps in the order of $10rpm$. How big of a speed difference the synchronizers are able to synchronize is the subject of this thesis. One of the considerations that is being taken into account for choosing how the ECU will synchronize speeds is that it is difficult to control the speed of the ICE precisely through the fuel intake [2]. If the synchronizers can only handle very small speed differences, that will likely leave little choice

but to use a second electric motor for the speed synchronization (the first one is for launch and torque filling). This is because electric motors can be controlled more precisely than ICEs [2]. On the other hand, if the synchronizers can handle larger speed differences, then controlling the ICE directly, imprecise as it may be, is a viable option without the need of a second electric motor in the transmission.

1.2 Synchronizers

1.2.1 General function in a transmission

A synchronizer, also known as synchromesh, is an important component of every transmission with discrete gear ratios. It makes it possible to engage and disengage moving gears smoothly while protecting the gears' teeth. Whether a transmission is manual or automatic, every gear associated with a different input-output ratio (i.e. first, second, etc.) sits next to a synchronizer. When each gear is selected during driving, the synchronizer first brings that gear up to speed and then meshes it, connecting the input power from the engine to the output of the transmission (to the wheels) through that gear. Figure 1-2 shows a schematic of this process.

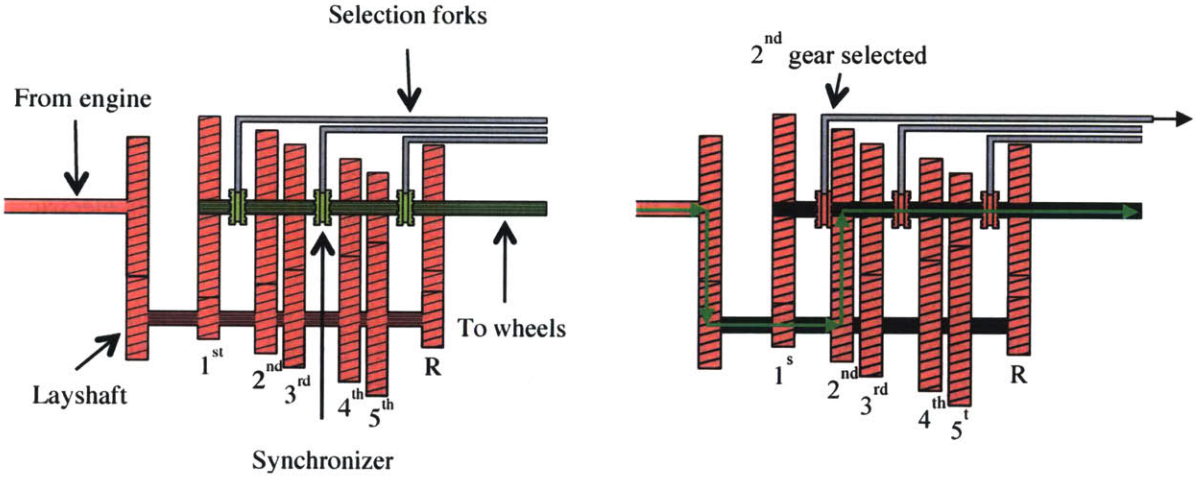

Figure 1-2: Schematic of the function of the synchronizer in a parallel shaft transmission
Components of the same color are rotating together. (a) No gear is engaged, the power from the engine is not transmitted to the wheels. (b) The synchronizer between first and second gear is used to select and engage second gear. The transmission of power is shown with green arrows.

There are several different types of synchronizers made by different manufacturers. Some of the most important types for gears in parallel shafts are the or Baulk-ring type (or Blocker ring type), typically used in manual transmissions, and the Pin-type (or Clark type), which are preferred for medium duty trucks applications because they trade off the drive feel for a higher brake capacity [4]. Others include the Lever-type, the Porsche type, and the Disk-and-Plate type [4], [5]. Each of these types describes a broad variety of subtypes and sizes. Their main differences are the mechanisms they use for engaging to start the synchronization and for locking once the synchronization is done. Nevertheless, except for the Disk-and-Plate type, they all have in common a moving part that is used for selecting gears, a mechanism (usually involving springs) for keeping the moving part from engaging with the gears unintentionally, and an interphase of

two or more conical surfaces that is responsible for the torque required for synchronization. This interface of conical surfaces is the core feature of the synchronizer. It allows for the synchronization of speeds between the shaft and a gear by converting an axial force into an equalizing torque between them. It is also the principal focus of this thesis as this interface is what determines the speed-matching potential of any synchronizer. The work presented here validates a mathematical model in consideration of the Baulk-ring type but is nevertheless extensible to the other types that also employ conical friction surfaces.

1.2.2 How a synchronizer works

In defining the capabilities and limitations of synchronizers in the new clutchless transmission, it is important to bear in mind the complete synchronization process. This process starts with the gear and output shaft rotating at different speeds with the synchronizer in the un-engaged position and ends with the gear and the shaft locked together through the synchronizer. Figure 1-3 depicts a Baulk-ring type synchronizer in the starting, un-engaged position.

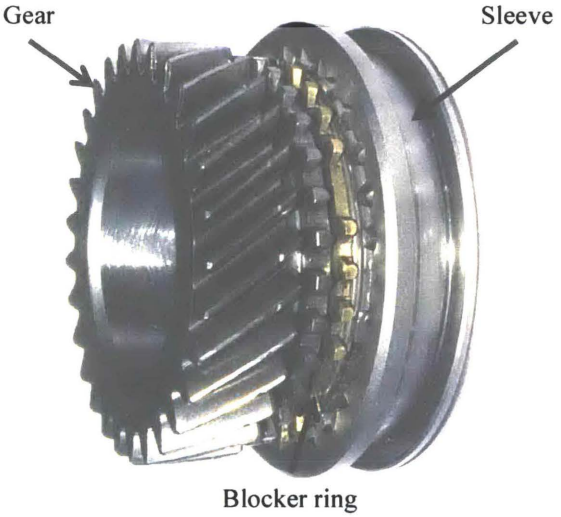

Figure 1-3: Baulk-ring type synchronizer and gear from a Honda vehicle
The picture shows the synchronizer in its un-engaged position. Both gear and synchronizer are assembled on the output shaft (not shown), but unlike the sleeve, the gear is not meshed to the shaft directly. In order for the gear to transmit the power it receives from the engine to the output shaft it has to be meshed from the side through the sleeve. The sleeve is actuated with a selection fork.

The following is an overview of the synchronization mechanism for the Baulk-ring type synchronizer. Considering one side of this Baulk-ring type, Figure 1-4 displays its components. Typically a synchronizer is bidirectional and therefore this picture would be symmetric with respect to the hub with a gear of different size on the other side (though there is only a single sleeve which slides in either direction). This specific synchronizer, which is also shown in Figure 1-3, is one of the two used for experimental validation of the mathematical model in Section 4. It is a particular kind among the Baulk-ring types in that it uses a wire spring instead of a strut detent for the pre-synchronization step. However, the function of the wire spring as a pre-synchronization element (see pre-synchronization phase below) is the same as that of the strut detent in other types.

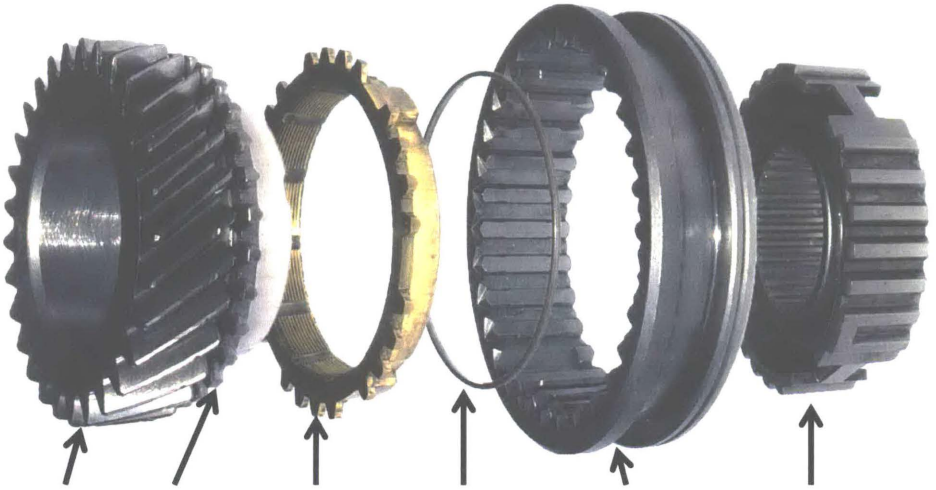

Figure 1-4: Components of a Baulk-ring type synchronizer with wire spring
From left to right, the gear sits in but is not meshed to the output shaft. The blocker ring, sits between gear and sleeve; its inner cone matches the conical side of the gear. The wire spring is used for pre-synchronization and indexing [6]. The sleeve allows the synchronizer to be actuated with the selection fork. The hub interlocks between the sleeve and the output shaft, allowing the sleeve to move axially and also providing the means for locking the assembly to the shaft.

The synchronization process can be described by the following 6 phases [1].

1. Neutral position
2. Pre-synchronization
3. Synchronization
4. Unlocking
5. Full engagement
6. Gear position assurance and torque transfer

Phase 1. Neutral position (Figure 1-5). The sleeve is centered on the hub and no axial force is exerted on it by the selection fork. The gear rotates freely independent of the rest of the synchronizer assembly. The detent, in this case the wire spring, prevents the sleeve from moving away from the center and starting the synchronization unintentionally. In this phase, a stop tab on the blocker ring that fits loosely inside a pocket on the hub (see Figure 1-5, right) allows the ring to rotate within a small space [4], though the rotation of the ring is unimportant in this phase. In figures Figure 1-5 through Figure 1-10 the reference frame is fixed with the hub and the gear rotates counterclockwise, i.e. in this frame the hub and sleeve do not rotate and the gear rotates in the direction of the arrow.

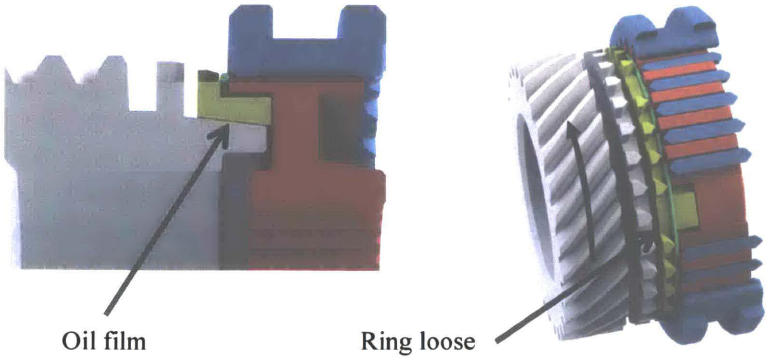

Figure 1-5: Synchronization phase 1–Neutral Position
The gear is free to rotate with the least amount of friction. The sleeve is in a centered position and the wire spring prevents it from moving towards the blocker ring. The blocker ring, wire spring, sleeve, and hub rotate together at all times.

Phase 2. Pre-synchronization (Figure 1-6). The initial axial displacement of the sleeve meets the wire spring and presses it against the blocker ring. With this initial axial force the ring inner cone makes contact with the gear cone and a friction torque is produced between them. The effect of this torque on the blocker ring side is that it makes the ring rotate (if it is not already there) within the hub pocket in the direction of the gear rotation until the stop tab prevents it from moving further. This is called indexing [5] because the tab stop is designed such that in this position the blocker ring teeth block the sleeve from engaging with the dog teeth of the gear [1]. On the gear side, the produced torque is applied towards slowing down the gear. Therefore, depending on the strength of the wire spring (or strut detent in other types) a small amount of synchronization happens at this stage [4]. When the axial force on the sleeve overcomes the resistance of the spring, the sleeve continues to move towards the blocker ring. This phase ends when the teeth of the sleeve make contact with the teeth of the blocker ring.

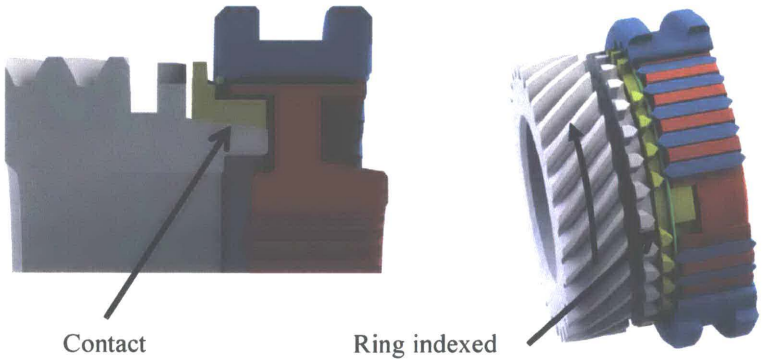

Figure 1-6: Synchronization phase 2–Pre-synchronization
When the sleeve initially moves towards the gear, it makes contact with the wire spring which pushes against the blocker ring. The friction cone surfaces come into contact activating the indexing action.

Phase 3. Synchronization (Figure 1-7). Once the flanks of the sleeve splines make contact with the blocker ring teeth, the axial force on the sleeve produces a friction torque on the gear that is

proportional to the force. The torque arises in the interface between the ring and the gear cone due to their coefficient of friction and their relative motion. This is referred to as synchronization torque [4] and it is what makes the gear slow down (or speed up) to the speed of the shaft. At the same time, the axial force on the sleeve produces on the ring an opposite torque due to the contact angle of the teeth flanks (see Figure 1-7 below, right). This is referred to as index torque and it is also proportional to the force [4]. The index torque produced, however, should be smaller than the synchronization torque as long as there is relative rotation of the gear with respect to the cone. The requirement that the index torque be smaller than the synchronization torque is called blocking safety [7] and is present throughout phase 3. Note that the action of the wire spring does not oppose anymore the motion of the sleeve (see Figure 1-7, left). In fact, in some designs for manual transmissions, the action of the detent is transformed at this stage into an additional axial force that aids in the shifting by means of ramps or boost surfaces [4].

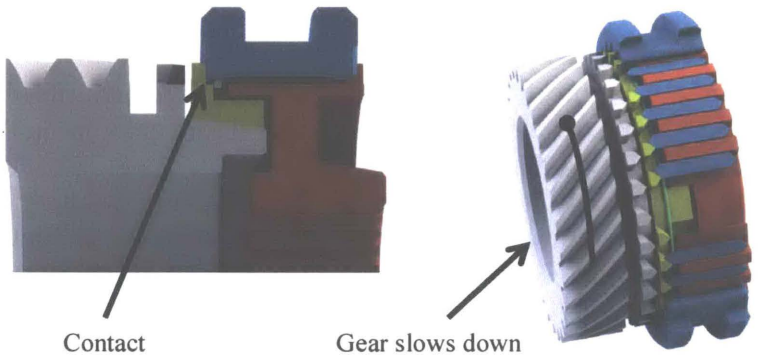

Figure 1-7: Synchronization phase 3–Synchronization
When the flanks of the sleeve splines come into contact with the blocker ring teeth, the synchronization torque is produced and the gear slows down. The indexed ring blocks further movement of the sleeve as long as there is relative rotation of the gear.

Phase 4. Unlocking (Figure 1-8). The synchronization torque, since it is dependent on the friction between the rotating parts, disappears once the synchronization is finished and both sides are rotating together. The index torque now dominates and makes the ring move out of the way of the sleeve splines [1]. Here the ring and the gear move together, with the ring stuck on the gear cone. This phenomenon is a thermal effect that occurs because in phase 3 the ring absorbs some of the energy dissipated as friction and suffers a slight diameter enlargement due to the temperature increase. When the friction diminishes, the ring "tries" to shrink back, but the axial force prevents it and it instead gets stuck on the gear cone. This is an important phenomenon that must be taken into account when designing the angle of the cones. While a small cone angle results in a higher synchronization torque for a given axial force, it also increases the force needed to unlock the ring at the beginning of phase 5. In fact, as shown in Eq. (5), in order to avoid permanent self-locking, the coefficient of friction between cones must be smaller than the tangent of the cone angle. The unlocking phase ends when the blocker ring completely clears out the way of the sleeve splines (see Figure 1-8, right), which can now continue to travel axially towards the dog teeth of the gear.

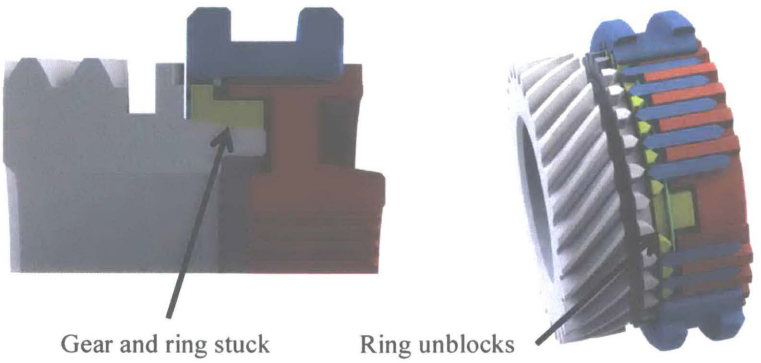

Figure 1-8: Synchronization phase 4–Unlocking
The synchronization is done and there is no relative rotation of the gear. The synchronization torque has disappeared and the index torque moves the blocker ring (now stuck to the gear) out of the way for the sleeve splines to come through.

Phase 5. Full engagement (Figure 1-9). With the blocker ring out of the way, the sleeve can now continue to move axially towards the gear dog teeth. Here, the angular position of the dog teeth is random with respect to the sleeve since it depends on the position at which the gear ended the synchronization phase. In general, the gear is not perfectly aligned (see Figure 1-9, right) and some rotation is required for the meshing to occur. Consequently, the sleeve spline flanks meet the flanks of the gear dog teeth and an increased force is now required to rotate the gear. This is termed "second load bump" because it is the second major increase in axial force during the synchronization process [4], [7]. Another factor that contributes to this increase in force is the self-locking phenomenon. The sleeve splines must align the teeth of the gear with those of the blocker ring, and this requires and extra force to unlock them first [4]. There is another possible scenario in this phase in which the ring is not stuck to the gear at the beginning of this phase. This may happen if the self-lock phenomenon never occurred (perhaps because the gear was already almost synchronized) or if at the end of the unlocking phase the torque difference between the two sides e.g. due to drag, is strong enough to unlock the ring [7].

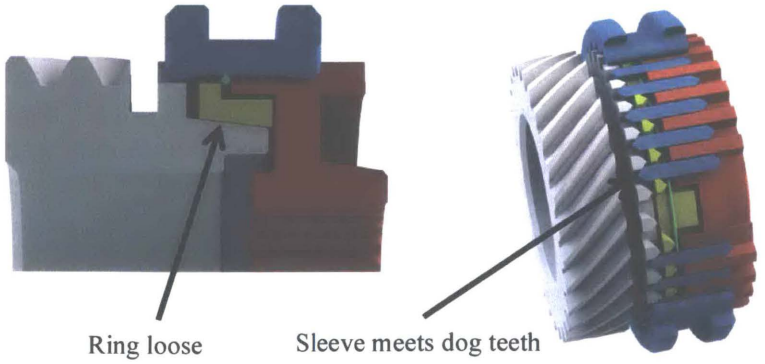

Figure 1-9: Synchronization phase 5–Full engagement
The sleeve travels axially and meets the dog teeth of the gear. But the gear is now stuck to the blocker ring, so there is an increase in the axial force needed for unlocking it. This phase ends when the sleeve splines align in between the gear dog teeth.

Phase 6. Gear position assurance and torque transfer (Figure 1-10). With the hub, blocker ring, and gear dog teeth now aligned, the sleeve finally moves to its final, in-gear position. Its displacement is normally limited by a stop between the sleeve itself and the hub (see Figure 1-4). At this point, torque is transferred by the gear via the dog teeth to the sleeve and further via the hub to the output shaft [1]. To prevent decoupling under load, both dog teeth and sleeve splines are back tapered such that the torque between them also keeps them meshed [7]. Synchronization is concluded when the sleeve reaches its final position.

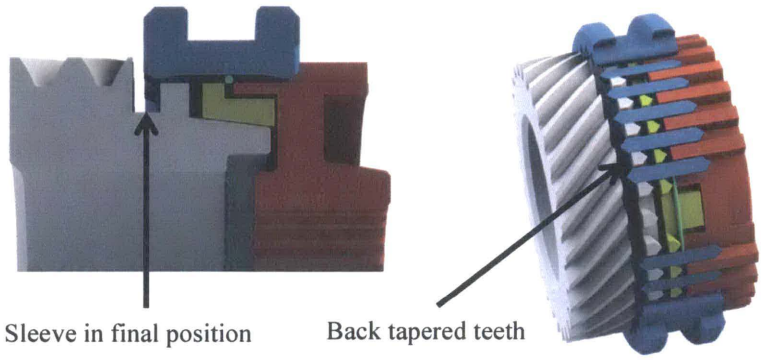

Figure 1-10: Synchronization phase 6–Gear position assurance and torque transfer
The sleeve moves to its final position and is prevented from moving further by stops between itself and the hub. Back tapers on the dog teeth and sleeve splines together with the transferred torque maintain the sleeve in this meshed position.

1.2.3 Literature on mathematical model

In order to determine a synchronizer's braking capacity for a given vehicle and transmission, its equations of motion must be determined. Considering the entire vehicle dynamics as the system to be modeled is complex and requires models of many subsystems that are not available. Nevertheless, literature shows that simplifications can be made without risk of losing the important system characteristics. According to Paul D. Walker and Nong Zhang, if the synchronization time is small, and the inertia of the target gear is significantly smaller than that of the vehicle, it is possible to model the synchronizer as a rigid body with the inertia of the components to be synchronized reflected on that target gear [8]. This is the case in the clutchless transmission project. The inertia of the components of the synchronizer itself is negligible in comparison to the inertia of the system. Accordingly, in the simulations presented here these inertias are neglected, and the experiment introduced in Section 2 is designed to validate this assumption.

The synchronization process is described in 6 different stages, thus there is also the question of which are the significant sub-processes that should be taken into account to accurately describe the overall system behavior. However, the focus of this thesis is to characterize the synchronizing potential and limitations of synchronizers in the configuration of the new clutchless transmission. Then, the most important questions that this work aims to answer for a given synchronizer are the following: 1, whether the synchronizer, based on its geometry and material and the system's physical properties and starting conditions, can synchronize the speeds of the system and how fast it can do so; and 2, whether the material that makes up the synchronizer is strong enough to withstand the forces present during shifting in the new

transmission. The first question can be answered by looking into phases 2 and 3 of the synchronization process because the completion of these phases implies that the synchronizer is adequate. The experiment introduced in Section 2 addresses this. Section 6 addresses the second question.

Taking a look at phases 2 and 3 of the synchronization process, it is evident that what dominates the synchronization time is the action between cone surfaces that arises when an axial force is applied on the sleeve. Depending on the strength of the spring force of the detent mechanism, a fraction of the synchronization happens during phase 2. By varying the spring constant in simulations, A. P. Bedmar shows that a bigger portion of the synchronization is done in phase 2 with increasing spring constant, but with little change in total synchronization time [4]. Moreover the source of the synchronization torque is the same in phase 2 and phase 3, so without loss of generality, the synchronization can be assumed to occur solely in phase 3.

With the previous two assumptions, the most important torques in the system are the synchronization torque, the index torque, and the drag torque [8]. In addition, there is friction between the sliding fork and the rotating sleeve, which is expected to have a small effect compared to the cone torque. Then, the following differential equations describe the system:

$$J_h\dot{\omega}_h = \tau_s - \tau_{D,h} - \tau_f \tag{1}$$

for the hub side, where J_h is the car inertia reflected on the hub side, ω_h is the angular velocity of the hub, τ_s is the synchronization torque, $\tau_{D,h}$ is the drag torque of the engine reflected on the gear and τ_f is the fork torque. And

$$J_g\dot{\omega}_g = -\tau_s - \tau_{D,g} \tag{2}$$

for the gear side, where J_g is the engine inertia reflected on the gear, ω_g is the angular velocity of the gear, and $\tau_{D,g}$ is the drag torque of the engine reflected on the gear.

The synchronization torque is the central focus. The inertias, angular velocities, and drag torques are inputs that depend on the system to be synchronized, but the synchronization torque must be designed to meet the desired performance. According to A. P. Bedmar, it is a function of the axial force on the sleeve, the friction coefficients at the cone interface(s), and the geometry of the cones, and is given by

$$\tau_s = F_f(t)\cdot\frac{\mu_c(t)\cdot R_c}{\sin\alpha_c}\left(1+\frac{1}{3}\left(\frac{b_c}{R_c}\right)^2\sin^2\alpha_c\right) \tag{3}$$

where F_f is the fork force on the sleeve, μ_c is the coefficient of friction between cones, R_c is the mean cone radius, α_c is the cone angle measured from the shaft axis, and b_c is the half length of the cone generatrix [4]. This applies to a synchronizer with a single cone. The factor in parenthesis accounts for the change in radius across the surface of the cone, but it makes an insignificant difference and is neglected [5], [7]–[9]. If additional cones are present, each cone contributes with a torque given by the same expression as Eq. (3), but if multiple cones are

employed in the design, they are expected to have similar geometry and material properties. Then Eq. (3) can be rewritten as

$$\tau_s = F_f(t) \cdot \frac{N_c \cdot \mu_c(t) \cdot R_c}{\sin \alpha_c} \tag{4}$$

for the general case with N_c cones [7]. As for the angle α_c, the smaller the value, the higher the torque it produces for a given force. But the constraint is that if it is too small, self-locking can occur as described in phase 4 of the synchronization. So the lower limit is

$$\tan \alpha_c \geq \mu_c \tag{5}$$

to prevent self-locking [7].

The coefficient of friction between cone surfaces, μ_c, is shown in Eq. (4) as a function of time because it changes slightly at the beginning of phase 3 when the oil film has not yet been broken and it is said to be in a mixed stage. This change in the value of the friction coefficient in the transition from hydrodynamic friction to solid friction is described by the Stribeck curve [4]. The simulation presented here neglects this edge effect because the mixed lubrication stage is assumed to last only a small fraction of the total synchronization time. Besides, all synchronizer rings are manufactured with grooves on the inside that are designed to break the oil film as fast as possible [9].

It has already been mentioned in the description of phase 3 that the synchronization torque must always be larger than the index torque, τ_I, while there is relative rotation of the gear with respect to the hub. This blocking safety condition is met by designing the flank angles of the teeth accordingly, such that $\tau_I < \tau_s$ [10] where τ_I is given by

$$\tau_I = F_f R_s \frac{1 - \mu_s \tan \beta_s}{\tan \beta_s + \mu_s}, \tag{6}$$

where R_s is the mean radius of the sleeve at the point of contact with the fork, μ_s is the coefficient of friction of the sleeve teeth, and β_s is the flank angle of the sleeve teeth. If the blocking safety is not met, clash between the sleeve splines and the gear dog teeth can occur [4], [7]. If it was not for this requirement, the flank angle β could be designed smaller and that would make self-locking less of a problem because the same index torque is used for unlocking the ring from the gear cone in phase 4. In addition, the index torque must be larger than the drag on the gear during phase 5 to ensure that the drag does not take over once the friction ring is inactive [4]. The following condition must therefore be met.

$$\tau_I > \tau_{D,g} \tag{7}$$

The fork torque that takes place between the selection fork and the rotating sleeve, τ_f, is given by

$$\tau_f = \mu_f F_f R_s, \tag{8}$$

where μ_f is the coefficient of friction between fork and sleeve. Lastly, the drag torques in Eqs. (1) and (2) are the reflected drag effects of the car and the engine on the hub and the gear respectively. Modeling drag torque precisely is complex as it has a high level of uncertainty and variability [8], but for the engine it can be approximated as being Coulombic [11] with the linear term proportional to the speed [4], [7], and for the hub side it can be estimated from the car drag (see Section 5.1).

2 Design of Experiment Setup

2.1 Purpose

Measuring a synchronizer's performance directly in the exact context in which it operates is complicated due to the complexity and inaccessibility of a vehicle transmission. Many aspects of a transmission that significantly affect the synchronization process such as vehicle and engine inertias, the drag generated by friction, thermodynamic effects [6], surface degradation [12] and vibration in the system are hard to model precisely. Nevertheless, the understanding of the basic mechanisms that dominate the behavior of the system as presented above permits to make approximations that can yield good estimates of the performance. The following experiment is designed to approximate the expected operating conditions of synchronizers in the clutchless transmission and monitor their performance given a set of known inputs. The results will make it possible to verify whether the analytical model of the system and the assumptions made above are valid for the clutchless transmission and to what extent.

2.2 Experiment requirements

The synchronizer is the object of the experiment, of course. The setup must allow for testing synchronizers of different sizes to ensure the results are generalizable. In addition, since lubrication is an important factor in the synchronization process, it must be included in the experiment. In order to emulate the engine inertia a flywheel with a large inertia is necessary. The flywheel represents the reflected inertia of the engine on the gear being synchronized. Also, it is important to model the drag of the engine, which is large. So the experiment should include a drag component. An axial force actuation mechanism is required for applying the input force on the sleeve fork while at the same time measuring this input force. The other two sensors needed are a tachometer for measuring the speed of the rotating components at all times and a timer for synchronizing the measurements and recording the time dependency of the process. The input variables to the system are the geometry and material properties of the synchronizer, the initial speed difference to be synchronized, the axial force exerted on the sleeve fork over time, and the inertia and drag of rotating components. The output is the synchronization time. Different values of the input variables need to be tested for the most reliable outcome.

2.3 Choice of setup and sensors

The experiment setup chosen is a manual lathe and is shown in Figure 2-1. The dynamic properties of a lathe fit the requirements that the experiment should implement a large inertia and include a drag component. Its versatility allows for mounting different sizes of synchronizers and shafts. The adjustability of the carriage makes it ideal for mounting different sizes of sleeve forks to provide the axial force for the different synchronizer sizes. Moreover, the ability of a lathe to change gear ratios between motor and spindle, provides a way of varying the inertia and drag of the system.

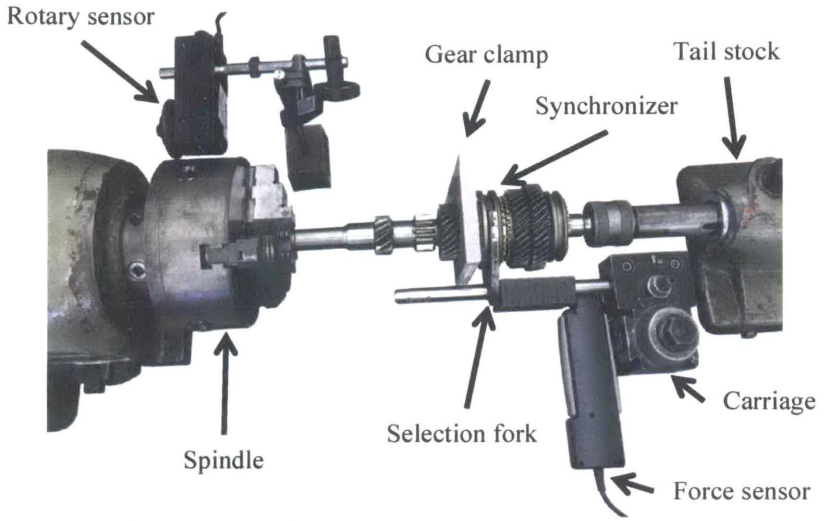

Figure 2-1: Lathe experiment setup for synchronizer engagement
The output shaft from a transmission is mounted between the spindle and the tail stock of a Monarch manual lathe. A custom clamp is used for restricting the rotation of the gear to be synchronized. The selection fork is mounted on the carriage such that the axial force can be measured with a force sensor. A rotary motion sensor measures the speed of the spindle.

The experiment is designed to obtain experimental data on synchronizers' braking performance to compare to and verify the mathematical model. It is executed by starting the spindle with an initial speed and then applying a known axial force to the sleeve towards the clamped gear, thereby bringing the speed of the spindle to zero. In general in a transmission, both the engine side of the synchronizer and the wheels side are rotating during synchronization. This will continue to be the case in the clutchless transmission. However, it is expected that the engine side of the synchronizer will have a relatively much smaller reflected inertia, meaning that the wheels side is not expected to noticeably change its speed. In fact, from the perspective of the comfort of a person in the vehicle, a perceptible deceleration of the car during an upshift (or acceleration during a downshift) is undesirable. So the approximation that one side of the synchronizer does not change speed during synchronization is adequate.

The fixed gear is a special case of a constant speed gear, but the speed difference between the two sides is the variable of interest. Hence, the experiment is representative of all the cases in which one side of the synchronizer has an approximately constant speed during synchronization. The only variable whose effect is different in the case of one side with a fixed, zero velocity with respect to the case of one side with a fixed, nonzero velocity is the drag torque. The drag torque, which is modeled as linear with velocity, has a larger impact at higher speeds. Nonetheless, the drag of a lathe is high even at relatively low speeds when the gearbox is engaged (see Section 3)

and therefore it has a significant effect on the synchronization experiment. It is expected, then, that the model validity extends to the more general case of two spinning sides.

Multiple experiments were performed under different configurations in the following steps: The gears and synchronizers are assembled onto their corresponding shaft in the transmission. The shaft is mounted in the spindle on one end and supported by a revolving tailstock spindle on the opposite end. For each different synchronizer tested, an aluminum clamp was fabricated to fix the rotation of the related gear. To prevent the clamp from over-constraining the shaft, it restricts the rotation only by means of an extension rod that rests against the lathe bed (not visible in Figure 2-1). The selection fork is mounted on the tool post via a loosely fitted sleeve on a tool holder such that the motion parallel to the shaft is unrestricted. This allows the force sensor to be placed between the carriage and the synchronizer sleeve so that the input force is transmitted through it. A rotary sensor is placed behind the spindle and making contact with it to measure its angular velocity. Both sensors are connected to a computer through a LabPro data collection interface.

Each experiment run consisted of first starting the spindle with some initial speed and second applying an axial force on the selection fork using the lathe carriage to engage the synchronizer until the spindle speed decreased to zero. The data acquisition was triggered by the sudden increase in the applied force. Two synchronizers of different sizes were tested, and for each one the inertia and drag of the lathe were varied from a minimum, with the spindle disengaged from the gearbox, to a maximum, with the gearbox engaged. Multiple runs were executed for each unique configuration to ensure repeatability. Additionally, a few runs were executed without adding oil to the synchronizer to investigate the extent of the influence of lubrication. In the cases with the gearbox engaged, the electric motor was used to give the initial speed difference and in the case of the gearbox disengaged, the spindle was started manually.

3 Parameter Determination

3.1 Experiment parameters

In order to evaluate the model speed vs. time curves for the same inputs as the experimental curves, all the input parameters in Eqs. (1), (2), and (4) must be determined first. These parameters are not always available and in some cases it is not possible to measure them directly. While the synchronizer geometry (R_c, b_c, α_c, and β_s) is measured directly using calipers, and the coefficients of friction between surfaces (μ_c, μ_s) can be found in commonly used tables such as [13], the drag coefficient and the inertia of the lathe must be measured indirectly. For this experiment they were measured from the lathe's time response to a known input torque, as shown in Figure 3-1. For each spindle configuration tested, the dynamic parameters were determined. The data was collected by pulling on a string wound several turns around the spindle. The pulling force is measured by a force sensor to calculate the torque input, while the speed is measured with a rotary motion sensor (see Figure 3-1). With the recorded data, the parameters are found assuming that the spindle behaves according to the following equation of motion:

$$J_{spdl} \cdot \dot{\omega}_{spdl} = \tau_{in}(t) - D_{spdl} \cdot \omega_{spdl} - \tau_{C,spdl}, \tag{9}$$

where J_{spdl} is the spindle inertia, ω_{spdl} is the spindle angular velocity, τ_{in} is the manually induced torque, D_{spdl} is the rotational drag coefficient of the spindle, and $\tau_{C,spdl}$ is the Coulombic drag torque of the spindle. Equation (9) is equivalent to Eqs. (1) and (2) except that in this case there is no synchronization torque. The drag torque is broken down into a linear component $D_{spdl}\omega_{spdl}$ and a Coulombic (static) component $\tau_{c,spdl}$. Therefore, there are three parameters that need to be found in order to model the system correctly. Those are the spindle inertia J_{spdl}, the linear drag coefficient D_{spdl}, and the Coulombic friction $\tau_{c,spdl}$.

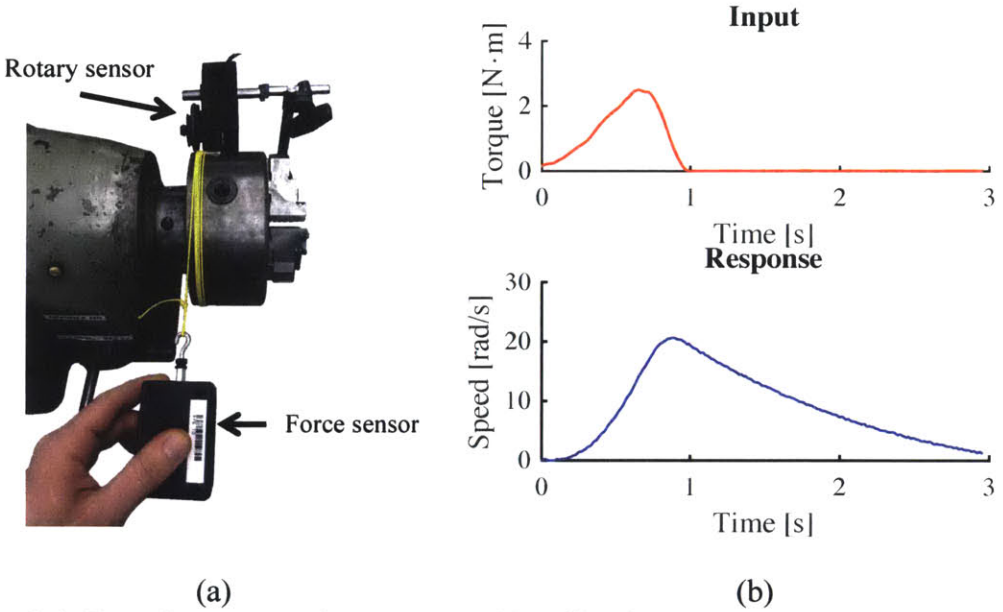

(a) (b)

Figure 3-1: Experiment setup for parameter identification
(a) Setup for parameter determination experiment. A known torque input is applied to the lathe spindle using a force sensor and a string wound several turns around it. A rotary motion sensor measures the spindle speed over time. (b) Experimental data for spindle parameter determination. Input torque (top) and speed response (bottom).

A simulator was created in Matlab (see Appendix A) to solve the above differential equation for the same input torque vector of the experiment to find the three desired parameters that minimize the mean squared error with respect to the experimental response (effectively "fitting" the model to the experimental data). Figure 3-2 shows the resulting fit and parameters for the same data as Figure 3-1 (b), which corresponds to the spindle disconnected from the gearbox.

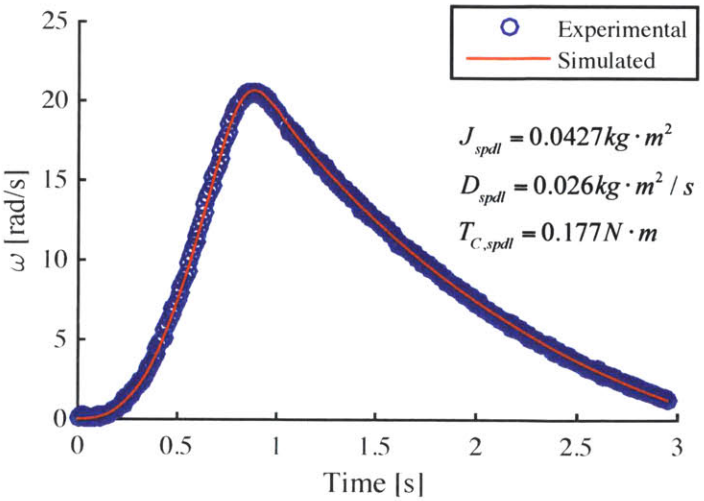

Figure 3-2: Simulated response of the spindle with optimized parameters
The experimental data is shown for the response of the spindle, disengaged from the gearbox, to a known, variable input torque. The speed increases up to about $1s$ when torque is present and then decreases due to drag. The values found for inertia, drag coefficient, and Coulombic torque are shown. The mean squared error for this fit is 1.5134.

For each configuration tested, multiple runs were executed and the parameters were found in the same manner. The results are given in Table 1 with 95% confidence interval.

Table 1–Dynamic parameters for configurations used in experiment

Parameter	J_{spdl} $(kg \cdot m^2)$	D_{spdl} $(kg \cdot m^2 / s)$	$T_{C,spdl}$ $(N \cdot m)$
Gearbox disengaged (low inertia and drag)	0.0429 ± 0.0002	0.026 ± 0.002	0.18 ± 0.01
Gearbox engaged (high inertia and drag)	0.0895 ± 0.0184	0.220 ± 0.003	2.07 ± 0.06

4 Evaluation of Experiment

Using the parameters found above and the model introduced in Section 1.2.3, a Matlab simulation was prepared (see Appendix B) for each of the different configurations of the experiment. The simulation was then compared to the experimental data to verify that the model is in agreement with the physical system and can be used to estimate synchronizer performance in a vehicle. Table 2 shows the relevant specifications of the synchronizers used in the experiments. The geometrical parameters where measured directly and the coefficients of friction were taken from [9] for the cones and from [14] for the sleeve.

Table 2–Description of synchronizers used in experiment

	Mean cone diam. (mm)	Cone angle (°)	COF cone (-)	Cone material	Number of cones	Mean sleeve diam. (mm)	COF sleeve
Synchro. #1	49.1	6.7	0.13	brass alloy	1	71.0	0.12
Synchro. #2	43.4	6.7	0.13	brass alloy	1	65.0	0.12

4.1 Simulation results

Figure 4-1 shows the simulation result from an experiment for the lathe configuration with the smaller inertia and with synchronizer #1; Figure 4-2 for the same lathe configuration but with synchronizer #2; Figure 4-3 for the larger inertia configuration and with synchronizer #1; and Figure 4-4 for the larger inertia configuration with synchronizer #2.

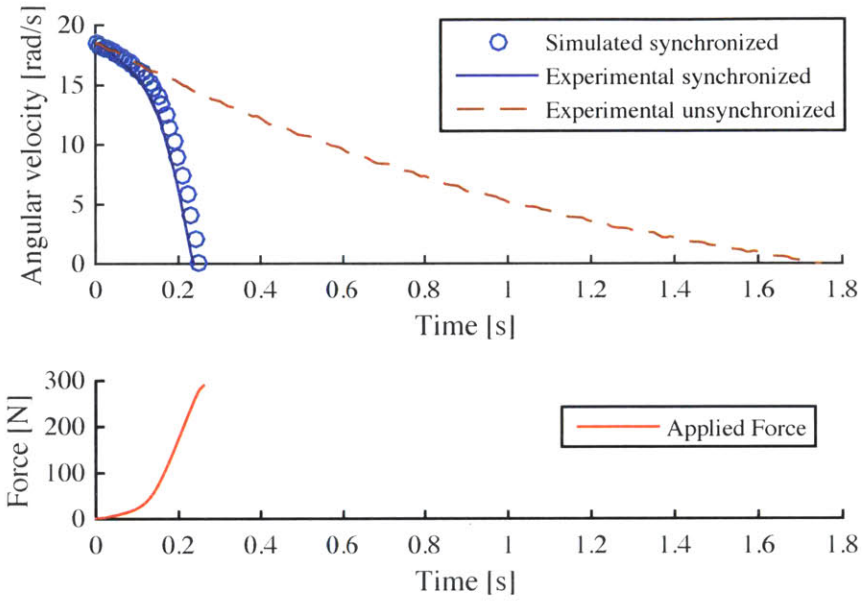

Figure 4-1: Small inertia experiment with synchronizer #1
(Top) The angular velocity of the spindle is plotted with respect to time for the unsynchronized and synchronized experimental data as well as for the simulated synchronization event. The unsynchronized data corresponds to the spindle slowing down due to its own drag. (Bottom) The corresponding input axial force on the fork is plotted.

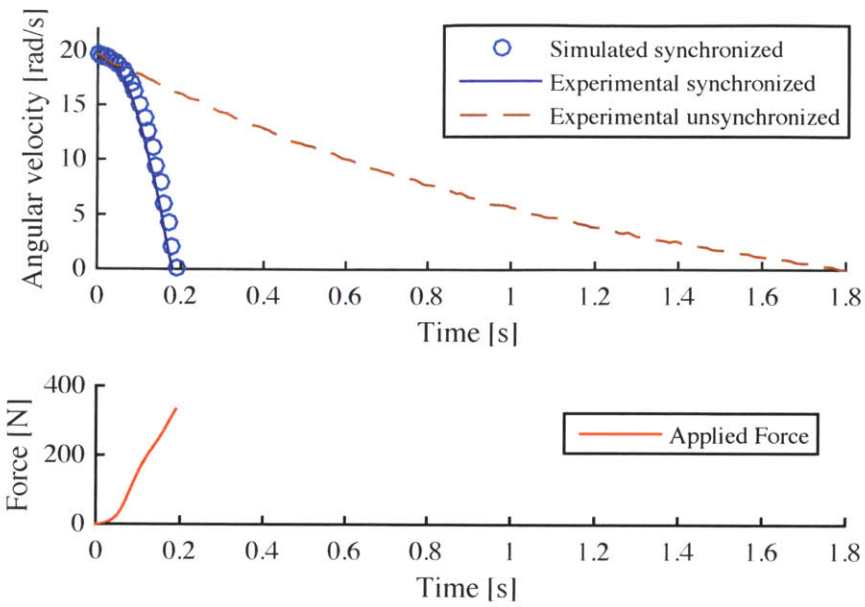

Figure 4-2: Small inertia experiment with synchronizer #2
(Top) The angular velocity of the spindle is plotted with respect to time for the unsynchronized and synchronized experimental data as well as for the simulated synchronization event. (Bottom) The corresponding input axial force on the fork is plotted.

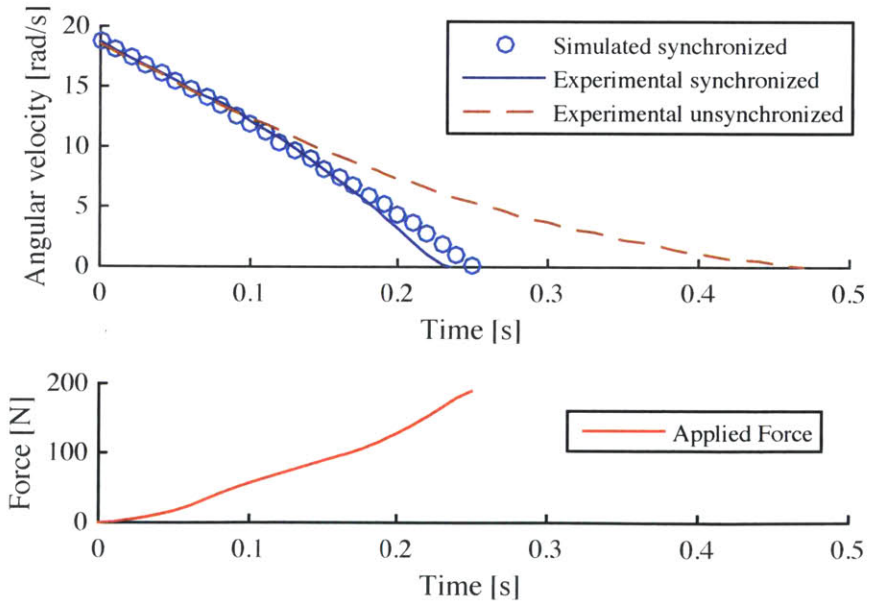

Figure 4-3: Large inertia experiment with synchronizer #1
(Top) The angular velocity of the spindle is plotted with respect to time for the unsynchronized and synchronized experimental data as well as for the simulated synchronization event. (Bottom) The corresponding input axial force on the fork is plotted.

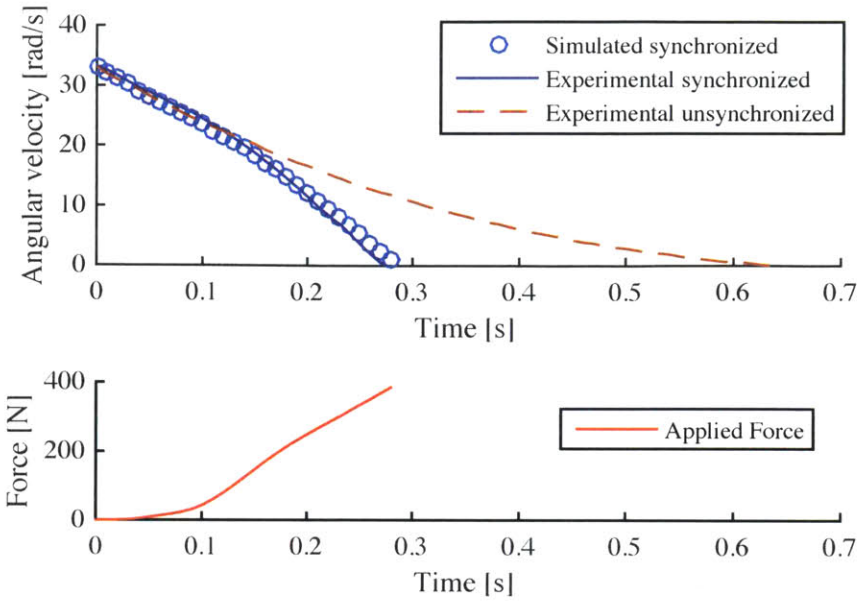

Figure 4-4: Large inertia experiment with synchronizer #2
(Top) The angular velocity of the spindle is plotted with respect to time for the unsynchronized and synchronized experimental data as well as for the simulated synchronization event. (Bottom) The corresponding input axial force on the fork is plotted.

4.2 Observations

These are some representative experiments of the 24 performed, all with similar results. Although every run is unique because the source of the force is manual (through the lathe carriage), these results show all the different configurations tested.

The diameter of the friction cone significantly affects the braking performance, in agreement with [4]. Comparing Figure 4-1 and Figure 4-2, it is evident that for a similar starting speed difference the synchronizer with the smaller diameter requires a substantially larger force to achieve a similar synchronization time.

The effect of the fork torque, which has been taken into account above, is small but not negligible. For example, not accounting for this torque in the case of a large inertia experiment with synchronizer #2 (Figure 4-4) results in an overestimation of the synchronization time by an extra 5%. This may or may not be significant depending on the desired accuracy. In this case, however, the synchronizers tested use only one friction cone, so the fork torque is expected to be less important in synchronizers with multiple cones.

Overall, the synchronization time tends to be slightly overestimated in the simulation with respect to the experimental data by up to about 7% (Figure 4-3). This may be a direct result of the uncertainty of the coefficient of friction of the cone surfaces and the fact that it is assumed to be constant in the simulation. Nevertheless, the results show that the proposed model does in fact describe well the most important characteristics of the synchronizing process. The model can

therefore be used to predict the performance of similar synchronizers in any transmission provided that the input parameters presented here are known.

5 Application in the Clutchless Transmission

In this section, the model validated above is used to estimate the performance of the available synchronizer in different possible scenarios in the clutchless transmission. The objective is to specify the relevant information needed for selecting and incorporating synchronizers in the new transmission. Normal operating conditions are assumed. Section 6 then gives an analysis of the possible extraordinaire conditions that may result in failure.

5.1 Parameters

5.1.1 Vehicle

In order to make predictions on synchronizer performance in a given transmission, the vehicle parameters must first be identified. The vehicle parameters of interest for a given upshift or downshift are the car and engine inertias and drags as reflected on the hub and the gear sides of the synchromesh. These principal parameters are represented in Figure 5-1.

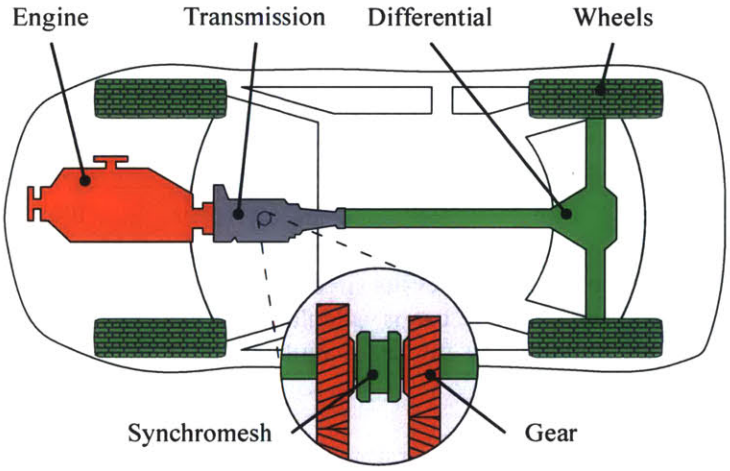

Figure 5-1: Schematic of the main inertial components
The most important parameters for the vehicle are the inertia of the engine, the inertia of the car as a whole, and their drags all reflected through gear ratios on the synchromesh. The inertia and drag of the engine (in red) is reflected on the gears depending on the gear ratio between them. The inertia and drag of the car and wheels (in green) is reflected on the shaft, and hence on the hub, through the differential.

The car inertia can be approximated from the mass of the car and the gear ratio between the output shaft and the wheels. So the reflected inertia from the car on the hub J_h is given [15] by

$$J_h = m_{car}\left(\frac{R_w}{r_{FD}}\right)^2 \tag{10}$$

where the ratio in parenthesis is the apparent radius of the wheels at the output shaft of the transmission, m_{car} is the mass of the car, R_w is the wheels radius, and r_{FD} is the final drive ratio between transmission output and wheels. The car drag accounts for the rolling resistance of the tires and the air drag. For the rolling resistance $F_{D,rr}$, the tires are approximated as equal and supporting an equal portion of the car's weight. It is given by the following equation [16]:

$$F_{D,rr} = \frac{C_{rr}(v_{car})m_{car}g}{1000} \tag{11}$$

where C_{rr} is the rolling resistance coefficient of the tires and g is the gravitational acceleration. The rolling resistance coefficient C_{rr} is a function of the speed of the vehicle v_{car}. From the data provided by the car manufacturer it can be described as linear as shown in Figure 5-2. The car tires are approximated to be all the same size and to contribute an equal amount of resistance.

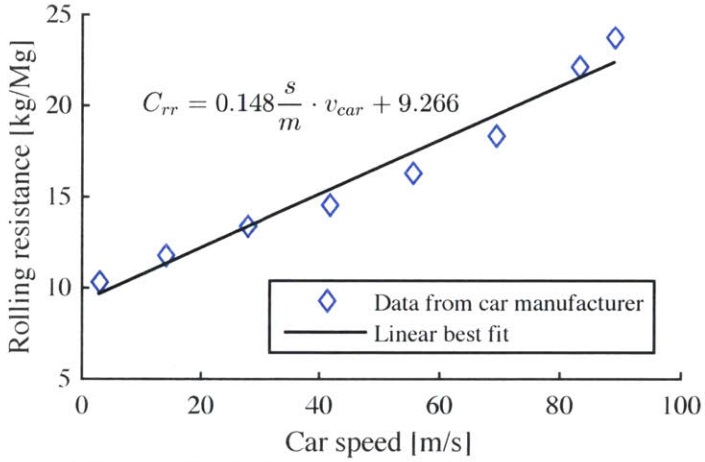

Figure 5-2: Rolling resistance of vehicle versus speed
The rolling resistance coefficient for the car is calculated for several speeds by averaging the front and rear wheel values provided by the car manufacturer. A linear to the data is made in order to make the calculations simpler.

The air drag coefficient C_x as well as the frontal area A_{car} are provided by the car manufacturer. And the air drag, $F_{D,air}$ is given by the following equation [17]:

$$F_{D,air} = \frac{1}{2}C_x\rho_{air}A_{car}v_{car}^2 \tag{12}$$

where A_{car} is the frontal area of the car and v_{car} is the car speed. Combining Eqs. (11) and (12) and using the same apparent ratio in Eq. (10), the total reflected car drag on the synchronizer hub is

$$\tau_{D,h} = \left[\frac{1}{2}C_x\rho_{air}A_{car}\left(\frac{\omega_h}{r_{FD}}R_w\right)^2 + 0.148\frac{s}{m}\left(\frac{\omega_h}{r_{FD}}R_w\right)\frac{m_{car}g}{1000} + 9.266\frac{m_{car}g}{1000}\right]\left(\frac{R_w}{r_{FD}}\right) \tag{13}$$

which simplifies to

$$\tau_{D,h} = \frac{1}{2} C_x \rho_{air} A_{car} \frac{R_w^3}{r_{FD}^3} \omega_h^2 + \left(0.148 \frac{s}{m}\right) \frac{R_w^2}{r_{FD}^2} \frac{m_{car} g}{1000} \omega_h + 9.266 \frac{R_w}{r_{FD}} \frac{m_{car} g}{1000} . \quad (14)$$

The engine inertia is provided by the car manufacturer. And the reflected inertia on the gear, J_g depends on the gear ratio selected. The following simulations are calculated for shifts between 1st and 2nd gear (the simulator in Appendix C is flexible to any shifts). If the gear ratio from the engine to the transmission output is r_{ET}, the reflected inertia on the selected gear [15] is

$$J_g = r_{ET}^2 \cdot J_E \quad (15)$$

where J_E is the engine inertia. The engine drag is not provided and is difficult to measure. For the predictions in this section, it was estimated from [18] where the friction power of a 4-cylinder engine is determined. It is assumed that the engine friction is proportional to the number of cylinders, so the calculated drag coefficient from the 4-cylinder engine is scaled up to the 8-cylinder engine of the vehicle in question. Reference [18] does not directly calculate a drag coefficient of the engine but instead they give the friction power at different engine angular velocities. The drag coefficient is calculated under the assumption that the friction power is the product of the average friction torque over the piston cycle and the angular velocity of the engine. It is also noted from [18] that the friction power can be approximated as linear with respect to engine speed, with a constant Coulombic component and a linear one. The vehicle parameters used in the predictions are then given in Table 3.

Table 3–Vehicle parameters used for synchronizer performance predictions

Parameter	Value
Car reflected inertia	$J_h = 7.2028\left[kg \cdot m^2\right]$
Car reflected drag	$\tau_{D,h} = 0.000137\left[kg \cdot m^2\right]\omega_h^2 + 0.01045\left[kg \cdot m^2 / s\right]\omega_h + 9.5982\left[N \cdot m\right]$
Engine reflected inertia	$J_g = 0.1052\left[kg \cdot m^2\right]r_{ET}^2$
Engine reflected drag	$\tau_{D,g} = 0.1526\left[N \cdot m \cdot s\right]r_{ET}\omega_g + 35.0141\left[N \cdot m\right]r_{ET}$

Before going into synchronization simulations, the engine behavior without any torque input other than its own drag is presented as a reference. Assuming that the engine starts at a speed ω_0 and is allowed to slow down by itself, using the estimated parameters in Table 3 the following is the expression for its speed over time.

$$\omega(t) = -229.45\left[\frac{rad}{s}\right] + \left(\omega_0 - 229.45\left[\frac{rad}{s}\right]\right) e^{-\frac{t}{1.38s}} \quad (16)$$

Figure 5-3 plots the engine speed from Eq. (17) over time starting at 9000*rpm* until it stops.

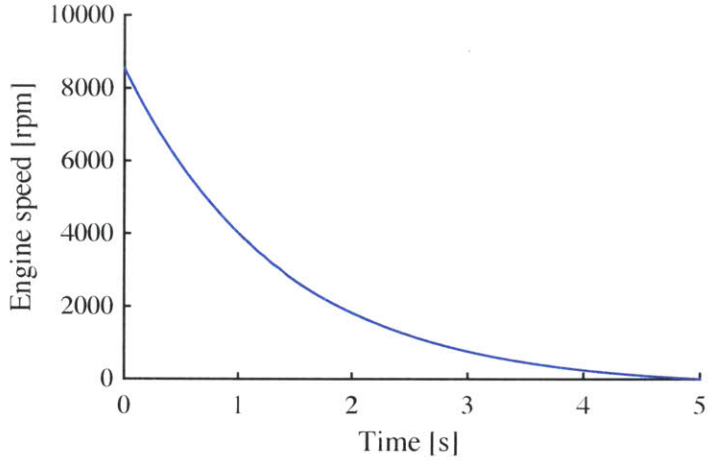

Figure 5-3: Engine slowing down by itself from 9000*rpm*
A significant load on the engine is its own drag. The plot shows the engine speed over time starting at 9000*rpm* according to the engine parameters estimated above.

5.1.2 Synchronizer

The device used for the following predictions was provided by the car manufacturer. It is of the Baulk-ring type with three friction cones, a mean cone diameter of 84.1*mm*, cone angle of 6.55°, a sleeve mean diameter of 112.17*mm* and a sleeve flank angle of 40°. The coefficient of friction, which in the model is assumed constant, was estimated from [6] and [19] where the time dependent friction coefficient is given for materials similar to that of the device used here. It is estimated from there to be $\mu_c = 0.10 \pm 0.02$. It is worth noting from [6] and [19] that although the friction coefficient of the synchronizer is not exactly constant, it varies very little throughout the synchronization event, confirming that the approximation of a constant coefficient of friction is valid.

5.2 Predicted synchronization time

The simulated synchronization event during an upshift from 1st to 2nd gear is shown in Figure 5-4. There, the initial engine speed difference to be synchronized is 500*rpm* and the fork force is 1500*N*. Throughout this section the car is allowed to change speed during the simulated synchronization process–that would be the case if a torque-filling feature is not implemented–so the car accelerates during upshifts and decelerates during downshifts. It is also assumed that the upshift begins with the engine at 9,000*rpm* and the downshift begins with the engine at 2,000*rpm*. However, as noted in Section 1.1.2, between the start of the shift and the point at which the synchronizer is activated, the engine speed changes considerably because it is expected to be adjusted first by the main synchronization mechanism (e.g. an electric motor). So the speed difference in the following figures is the difference between what the engine speed should be at the end of synchronization (if the car didn't decelerate or accelerate) and what it is when the synchronizer is activated. For example, Figure 5-4 represents the portion of the synchronization done by the synchronizer during an upshift where the engine started at 9,000*rpm* and needed to decelerate from that speed to about 6,400*rpm*. But in reality the engine has already slowed down to about 6,900*rpm* by the time the synchronizer is activated, and when the process

is complete the engine speed is slightly above 6,400*rpm* (because in this case the car was allowed to speed up). Hereinafter, "synchronization time" refers to the time period starting at engagement of the selection fork until the speeds of the engine side and the wheels side are the same. This is different from "shift time," which may include synchronization by another mechanism.

In addition, this section assumes that only the synchromesh is used for synchronization since the purpose of this work is to study the capabilities of the synchromesh. However, in reality the engine throttle or an electric motor may be used to assist in this process.

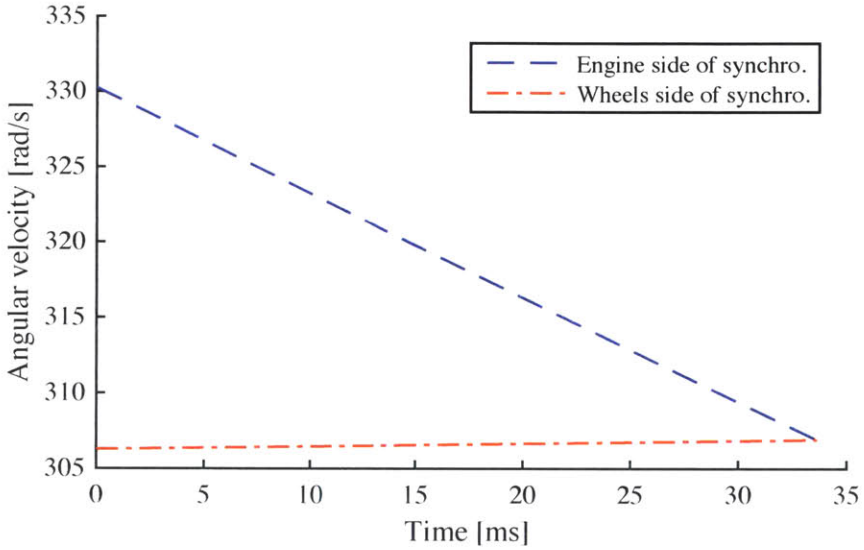

Figure 5-4: Synchronization event during an upshift from 1st to 2nd gear
At time zero, when the speed deficit of the engine is 500*rpm*, the synchronizer is activated. The action of the friction cones then slow the engine down and speed the wheels up until around 34*ms* the selected gear and the shaft are rotating together, at which point the process is finished. An upshift from 1st to 2nd gear is assumed with 1500*N* of fork force, the engine initially at 9,000*rpm* and the vehicle parameters given in Table 3.

5.2.1 Varying speed to synchronize and fork force

One of the main determinants in choosing a synchronizer for a particular transmission is the speed difference that it can handle and the fork force necessary for it. The following figures display the synchronization time for a range of initial engine speed deficits from 0 to 500*rpm*. Figure 5-5 shows the simulated synchronization times during an upshift for a range of selection fork forces. Figure 5-6 shows the simulated synchronization times during a downshift for the same configuration.

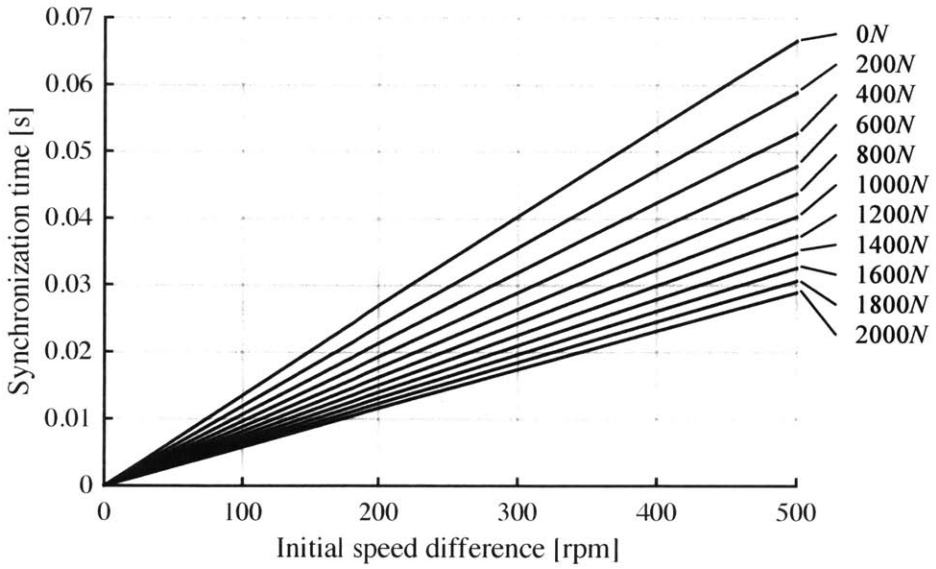

Figure 5-5: Upshift synchronization time for varying speed to synchronize and force
The figure shows the synchronization times during an upshift from 1st to 2nd gear. The horizontal axis represents the difference between the engine speed when the synchronizer is activated and what it should be at the end of synchronization. The time goes down with increasing fork force.

An important result from the upshift simulation is that even if the fork force is zero (meaning that the synchronizer is never activated) the synchronization is completed naturally. The reason for this is the drag torque of the engine. Under its own drag and in the absence of any other torque, the engine slows down faster than the wheels do. Hence, since during an upshift the engine must slow down, its drag torque helps.

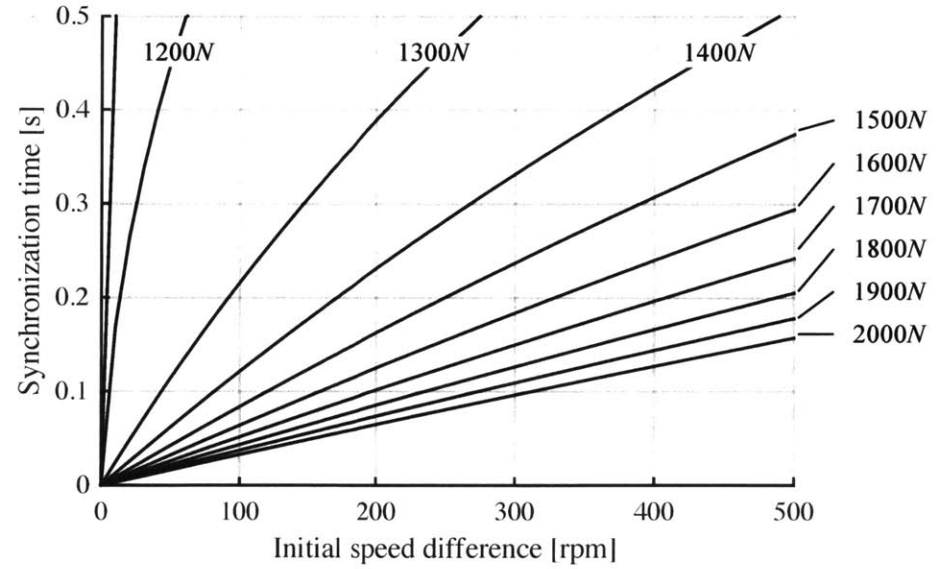

Figure 5-6: Downshift synchronization time for varying speed to synchronize and force
The horizontal axis represents the difference between the engine speed when the synchronizer is activated and what it should be at the end of synchronization. The time goes down with increasing fork force.

5.2.2 *Varying speed to synchronize and engine speed at start of shift*

It is clear from Figure 5-6 that the process takes much more braking power during a downshift than during an upshift. For that reason, Figure 5-7 shows the dependence of synchronization time on starting engine speed, which is related to drag.

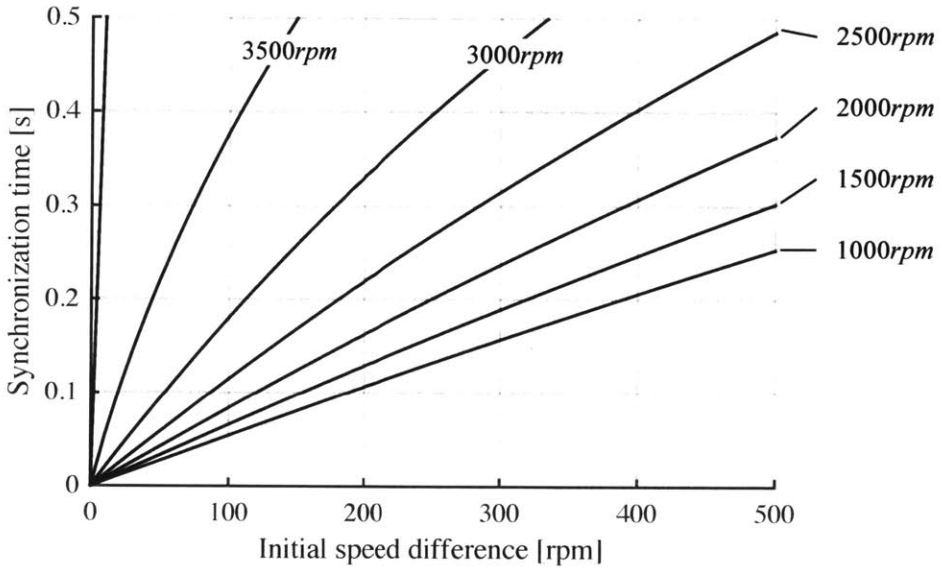

Figure 5-7: Downshift synchronization time for varying initial engine speed
The horizontal axis represents the difference between the engine speed when the synchronizer is activated and what it should be at the end of synchronization. The time goes up with increasing starting engine speed due to drag. The fork force is assumed to be 1500*N*.

The engine drag must be overcome and the engine accelerated for a downshift. This effect is amplified for higher starting engine speeds due to the dependence of drag on engine speed. Figure 5-7 plots the same downshift as in Figure 5-6 gear but for a constant force of 1500*N* and varying starting engine speed.

5.2.3 *Varying speed to synchronize and synchronizer size*

Over the same range of engine speed deficits, varying the mean diameter of the cone rings affects the synchronization time, a fact that is expected from Eq. (4). The larger the diameter of the cones the smaller the synchronization time for the same force. Figure 5-8 shows the synchronization time during an upshift for different cone diameters and for a fork force of 1500*N*.

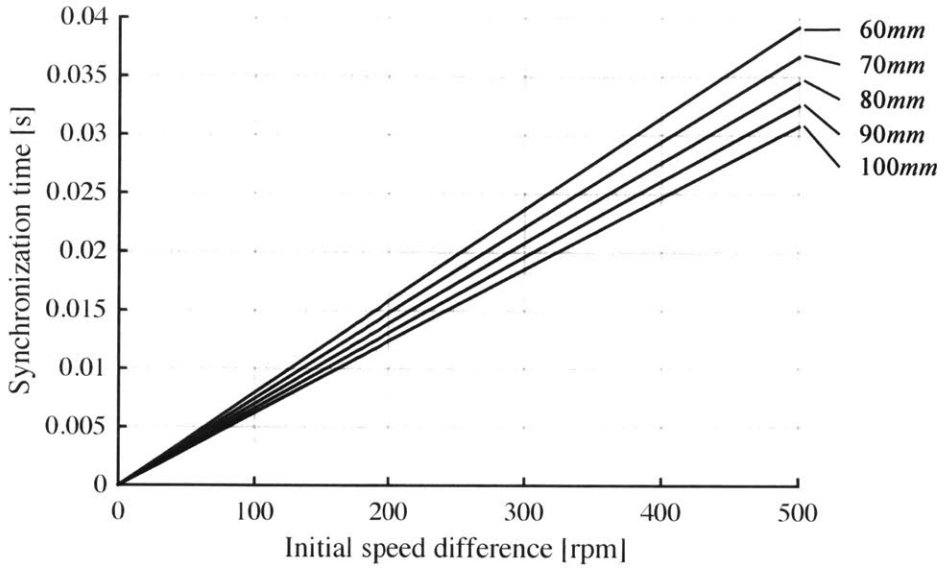

Figure 5-8: Upshift synchronization time for varying mean cone diameter of synchronizer
The synchronization time is shown for different mean cone diameters over a range of starting engine speed difference from 0 to 500*rpm* and for a fork force of 1500*N*. Increasing the cone diameter reduces the synchronization time.

Although during an upshift the synchronization time is already small without the action of the synchronizer, Figure 5-8 shows that varying the mean cone diameter has a significant impact. By increasing for example the mean cone diameter from 60*mm* to 100*mm*, the synchronization time is reduced by 23% for any starting engine speed difference.

5.2.4 Varying number of friction cones

One limitation of increasing the cone diameter is that the device becomes larger and at some point it becomes unfeasible to continue increasing the cone diameter because of space and/or weight restrictions. In practice, a better way to increase braking performance for a given fork force is to increase the number of friction cone surfaces [7]. Figure 5-9 shows the synchronization time during an upshift for some common number of friction cone surfaces. In general, more cones means much higher complexity of the synchromesh. According to Schaeffler KG, quadruple-cone synchronization system are starting to be implemented in isolated cases [9].

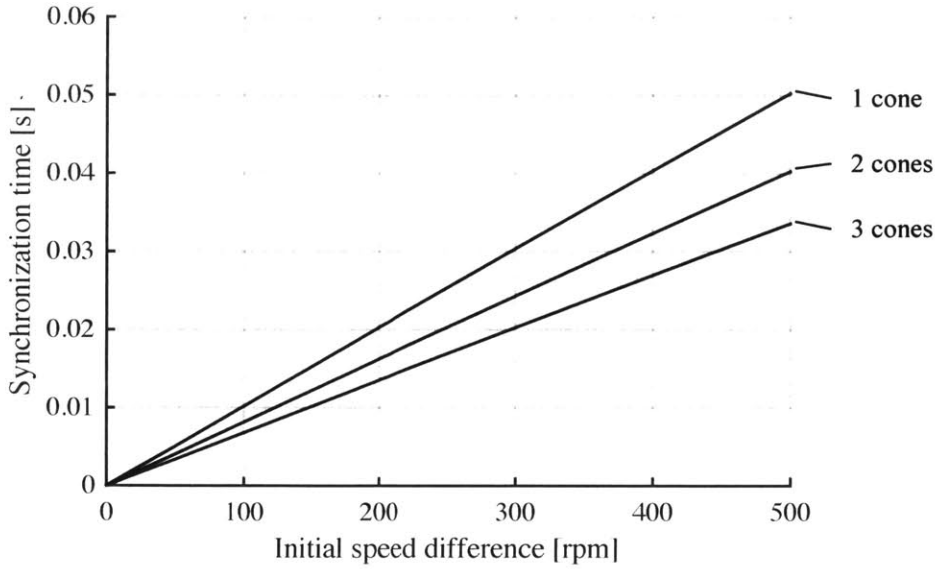

Figure 5-9: Upshift synchronization time for varying number of friction cones
The number of friction cones greatly affects the performance of the synchronizer. The figure shows the synchronization times for different number of cones, a fork force of $1500N$, and a mean cone diameter of $84.1mm$.

5.2.5 Varying speed to synchronize and coefficient of friction

The cone surfaces' coefficient of sliding friction is the source of the synchronization torque. Figure 5-10 shows the synchronization time for different coefficients of friction.

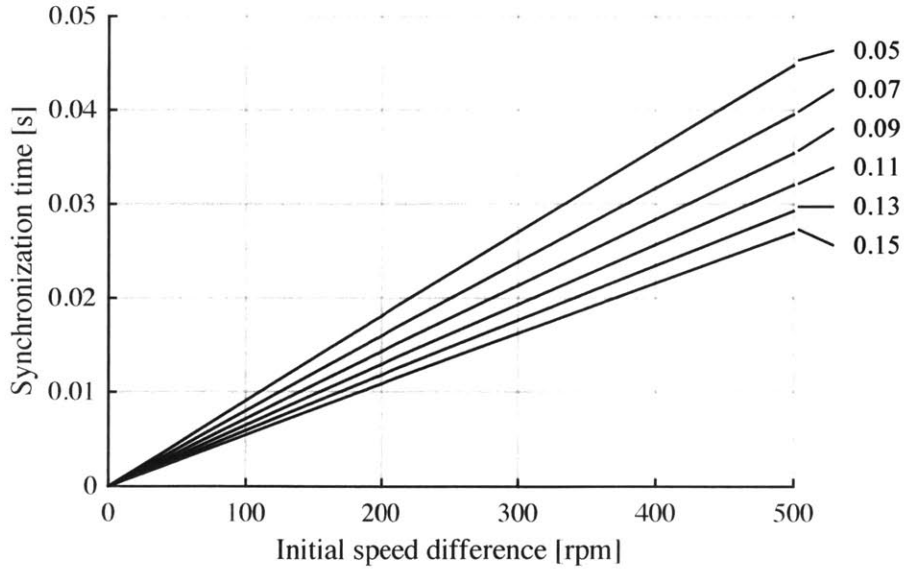

Figure 5-10: Upshift synchronization time for varying cone coefficient of friction
The synchronization time increases with decreasing cone coefficient of friction, which occurs due to wear of the cone surfaces either naturally from extended use or from misuse. The figure shows the synchronization time for a fork force of $1500N$ and varying coefficient of friction.

A lot of research has been done to design materials or surface linings to achieve better friction coefficients without decreasing the durability of the friction rings. The friction coefficient also decreases with increasing wear on the cone surfaces, damaging the synchronizer performance.

6 Failure Modes

Because of the nature of the large forces and energy dissipation that synchronizers are subject to it is important to consider the events that may result in malfunction. Whereas the previous results are valid for synchronizers in normal operating conditions, this section explores the different conditions that may lead to failure or damage.

6.1 Shearing

One possible failure mode that was considered given the large inertias that the synchromesh is expected to bear in the clutchless transmission was shearing of the blocker ring teeth. During the synchronization process the fork force is transmitted from the sleeve to the cones through the small teeth of the blocker ring described in Section 5.1.2. The blocker ring must therefore be able to withstand that force without yielding or deforming. In order to determine the limiting axial force for which the blocker ring will not yield, finite element analysis (FEA) was done on the ring using SolidWorks. A Rockwell hardness test on the ring was used to estimate the material strength. The measured ultimate tensile strength of the material from the Rockwell test was $640 \pm 10 MPa$. Based on this value, the yield strength (the value of equivalent stress at which a material starts to permanently deform [20]) of the metal is estimated to be around $400 MPa$. Figure 6-1 shows a portion of the synchromesh during the FEA analysis. The colors indicate the equivalent tensile stress (von Misses stress) throughout the part.

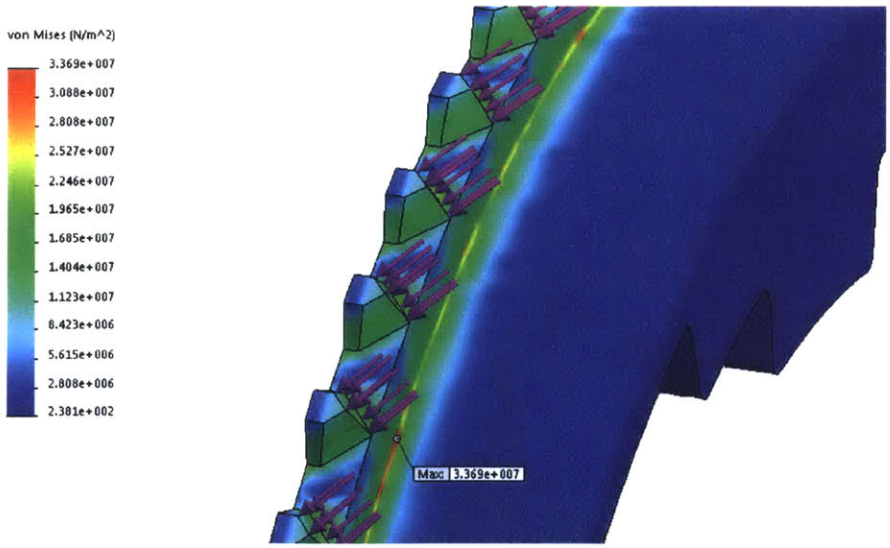

Figure 6-1: FEA performed on the synchronizer ring used in the simulations
The FEA analysis of the synchronizer ring shows the levels of stress on the material for a given applied force. Here, the force being applied is $1500N$ and it is applied uniformly on all the right flanks of the ring teeth. The ring is fixed from the inside of the cone as it would be during synchronization. In this case, the maximum equivalent stress induced is $33.69 MPa$.

For the load applied in Figure 6-1 the maximum stress on the material is 33.69*MPa*, which is considerably lower than the material yield strength, meaning that the material will not yield for the 1500*N* force applied. In order to determine the force for which the ring would start to deform, FEA analysis was performed for increasing forces on the synchronizer ring used in the simulations. A plot of the maximum stress as a function of the force applied is given in Figure 6-2.

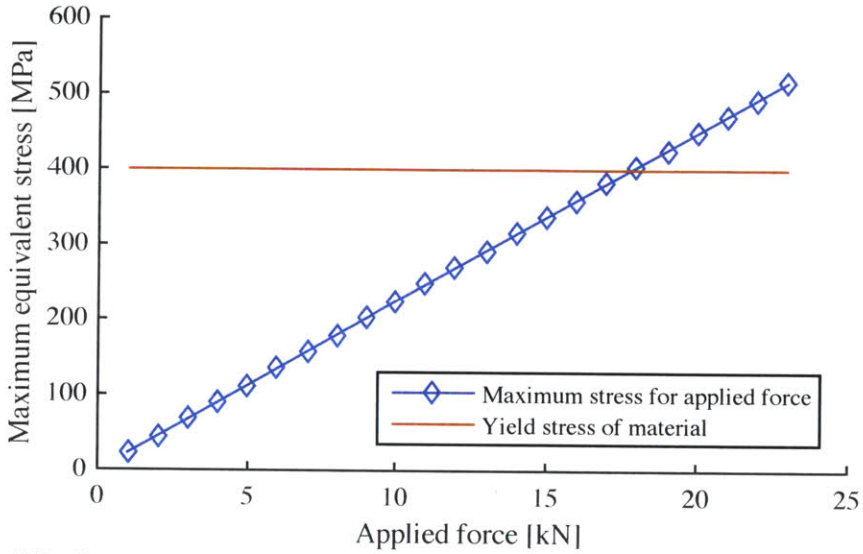

Figure 6-2: Maximum ring stress from FEA as function of force applied
The maximum equivalent tensile stress induced on the ring from FEA is plotted against the fork force applied. The plot shows that the material would not yield unless the force is around 17,800*N* or larger, which is considerably larger than the nominal fork force of 1500*N*.

Figure 6-2 shows that the ring would start to yield around 17,800*N*, that is one order of magnitude larger than the nominal 1500*N* force for these rings. Even though there is uncertainty in the determination of the yield strength of the metal, this reveals that as far as material strength is concerned, the fork force can be increased with respect to the nominal value if needed to adapt to the clutchless transmission. This result suggests that shearing of the teeth is not the failure mechanism that limits the axial force to the 1500*N* range.

6.1.1 Shearing and tire slip

In order to put the above force values in perspective, a comparison is made with the maximum torque that the wheels can take before they lose traction and slip. For the vehicle considered here, this effect occurs around 4371*Nm* of torque at the wheels according to the manufacturer. The torque at the synchromesh that would induce that torque on the wheels is 816.4*Nm* (neglecting the inertia of the drivetrain components), which corresponds to 7382.0*N* of fork force. That means that although taking into account the drivetrain inertia would allow for a larger force, the tires would slip before the limiting material strength of the blocker ring is approached. Figure 6-3 makes this comparison by plotting the simulated synchronization events for a range of torques highlighting the critical values.

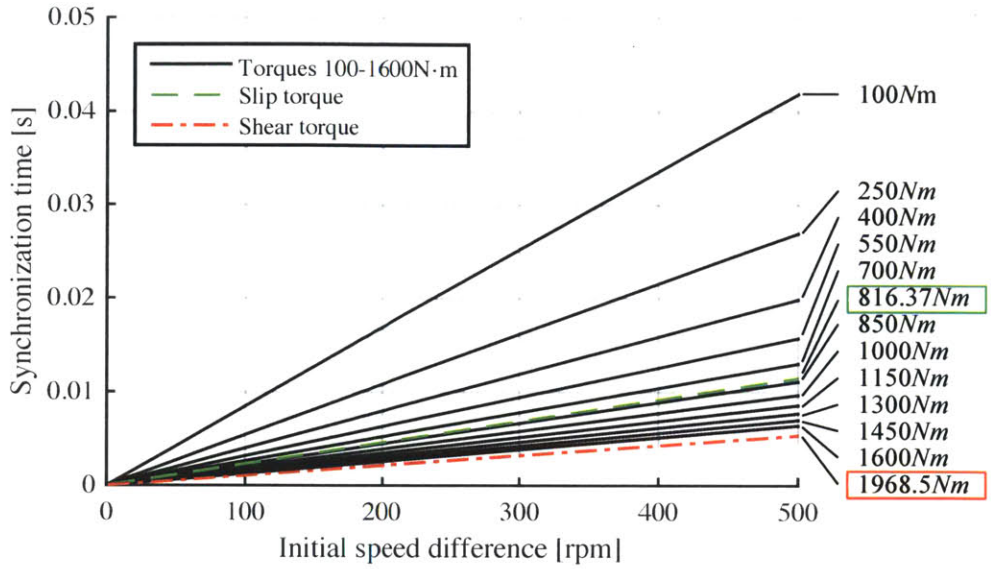

Figure 6-3: Critical torque values for wheel slip and shearing of teeth
Critical synchronization torque values during an upshift from 1st to 2nd gear starting at an engine speed of 9000*rpm*. The synchromesh torque that would induce wheel slip during synchronization is much smaller than the torque that would be exerted near the material strength of the ring. A fork force of 7382.0*N* would create a torque of 816.37*Nm* making the tires slip. And a force of 17.8*kN* would create a torque of 1968.5*Nm* but the dog teeth of the ring would start to break.

6.2 Clash

Clash refers to the collision of sleeve with gear dog teeth in the event that the sleeve moves towards the gear before the speeds have been synchronized. Clash is evidently a problem because it causes the sleeve and gear teeth to grind together and significantly reduce their lifespan. The main cause for clash to occur is when the blocking safety is not met, and this can happen for a number of reasons including high wear of the cone surfaces, overheating, high oil viscosity, and low coefficient of friction [7].

6.2.1 High wear, overheating, and low coefficient of friction

One of the most common malfunctions of synchronizers is wear of the friction surfaces. Wear happens slowly in normal working conditions. Ideally the coefficient of friction of the cones would not change over time. But in reality, since the friction torque comes from contact between solid surfaces, the surfaces degrade over time and the coefficient of friction decreases [7]. Ref. [12] shows that for a manual synchronizer the coefficient of friction decreases with the number of shifts, with clash occurring around 40,000 shifts. When the rings are new, the coefficient of friction is high because the roughness of the surface easily removes the oil film for the solid surface to come into contact. But as the surfaces wear their roughness decreases and it becomes harder to remove the oil film. When the oil film is not removed completely, friction comes about from a combination of fluid friction and solid contact, but the fluid friction is considerably lower and therefore the overall friction is lower [12].

Wear can arise quickly if the operating conditions are not adequate. According to [9], minimal contact with abrasive media produces grooves on the ring surface. But it can also occur due to overheating of the friction rings [7]. The heat comes from the energy dissipated by the friction torque. Therefore, the rate of energy dissipation per unit area of friction surfaces in the clutchless transmission should be comparable to that rate for current transmission. This hypothesis is made under the assumption that synchronizers in current transmissions operate just under the limit (with a safety factor) of energy dissipation rate that is healthy. There is otherwise little incentive to employ larger, heavier, and more expensive devices. Ref. [21] lists a range of energy dissipation rates per unit area for all possible shifts in a manual transmission of a medium-size passenger car. The values range from $0.09 W/mm^2$ for an upshift from 1st to 2nd gear in which the driver applies a force of $22N$ on the shift lever to $0.45 W/mm^2$ for an upshift from 2nd to 3rd gear in which the driver applies a $67N$ force on the shift lever.

The energy change in all components during a shift event are accounted for in the calculation of the specific energy dissipation rate. Figure 6-4 shows a schematic of the energy flow for the synchronization during an upshift.

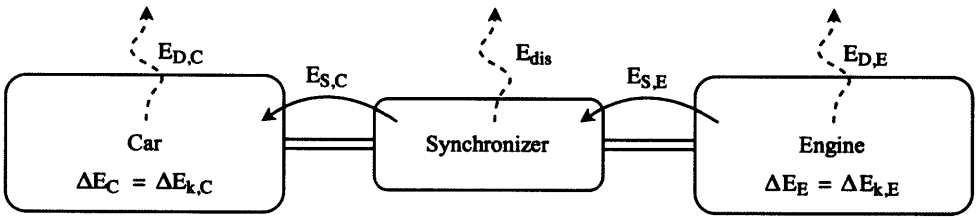

Figure 6-4: Schematic of the energy flow during synchronization
The energy flow through the synchronizer is calculated from the difference between the energy coming from the engine and the energy delivered to the car during an upshift. The total change in energy of the car and engine is equal to their respective change in kinetic energy, which in turn results from both drag torque and synchronization torque.

The energy dissipated is calculated from the difference between the energy taken from the engine and the energy delivered to the car according to the following equation:

$$E_{dis} = E_{S,E} - E_{S,C} \tag{17}$$

The energy coming from the car $E_{S,E}$ is equal to the negative change in its kinetic energy $\Delta E_{k,E}$ minus the energy it loses to drag $E_{D,E}$. The energy delivered to the car $E_{S,C}$ is equal to its change in kinetic energy $\Delta E_{k,C}$ plus the energy the car loses to drag $E_{D,C}$. The energy lost to drag is calculated by integrating the product of drag torque and the angular speed:

$$E_{D,E} = \int_0^{t_f} \tau_{D,g} \omega_g \, dt \tag{18}$$

and

$$E_{D,C} = \int_0^{t_f} \tau_{D,h} \omega_h \, dt \tag{19}$$

The energy dissipated by the synchronizer is then

$$E_{dis} = \left(-\Delta E_{k,E} - E_{D,E}\right) - \left(\Delta E_{k,C} + E_{D,C}\right). \tag{20}$$

This quantity is then divided by the total friction area of the cones and by the synchronization time to find the energy dissipation rate per unit area. Table 4 lists the calculated values for an upshift from 1st to 2nd gear starting at 9000*rpm* for a range of fork forces. These values are calculated from a simulation using the parameters in Table 3.

Table 4–Specific energy dissipation rates versus fork shift force

Force (k*N*)	1.0	1.1	1.2	1.3	1.4	1.5	1.6	1.7	1.8	1.9	2.0
Specific energy dissipation rate (W/mm^2)	0.47	0.51	0.56	0.61	0.65	0.70	0.75	0.79	0.84	0.89	0.93

These values of energy dissipation rate per unit area of friction surface are higher than those from [21] but they are comparable to the $0.45 W/mm^2$ from literature. Considering that this is not intended to be used in a manual transmission, it is likely safe to permit slightly higher values because a large safety factor would not be needed. Nevertheless, since the wear of the friction surfaces appears more rapidly at higher temperatures, it is essential to keep the energy dissipation rate as small as possible.

On the other hand, according to Eq. (7) the force must be such that the index torque τ_I is higher than the drag reflected on the gear $\tau_{D,g}$ during phase 5 of the synchronization to ensure the completion of the shift. Hence, the force matters for two different reasons at two different stages. Figure 6-5 shows the two stages at which the force must meet two different requirements.

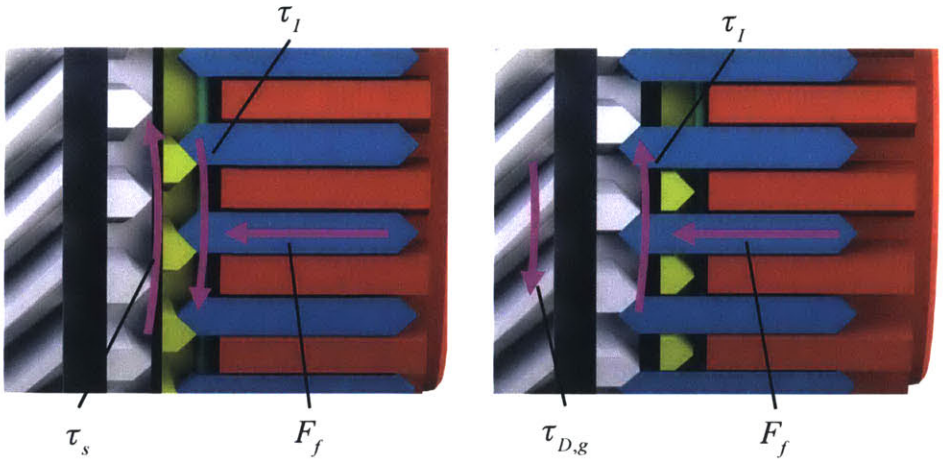

Figure 6-5: Two different considerations for the axial force
(a) During phase 3 of the synchronization the axial force F_f must be such that the torque produced can match the speeds of the two inertias but the limitation is that forces above a certain threshold can damage the cone surfaces due to the high energy dissipation rate per unit area of friction surfaces. (b) During phase 5 the index torque induced by F_f must be larger than the drag reflected on the gear so that full engagement is possible.

Figure 6-6 shows a plot of the minimum force required to ensure full engagement for a range of target engine speed during every possible shift.

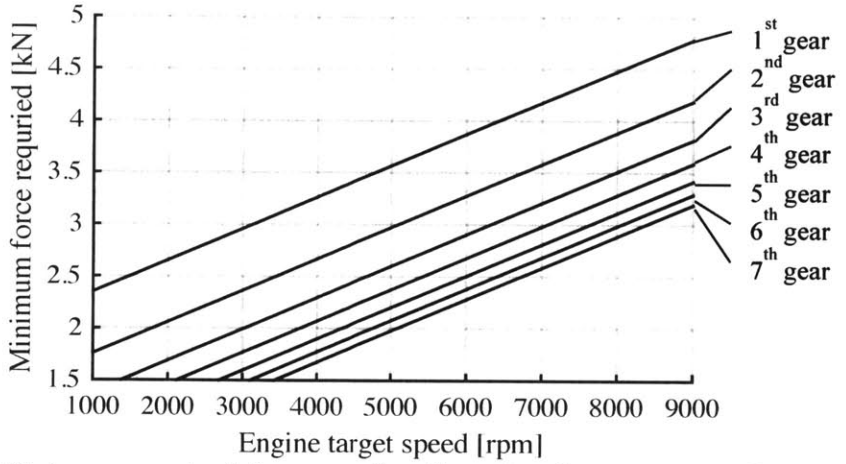

Figure 6-6: Minimum required force as a function of engine target speed
To ensure that the shift can be completed after the synchronization phase, the index torque must be greater than the reflected drag on the gear. Otherwise the drag torque may prevent the sleeve from meshing in between the gear dog teeth. The figure shows the minimum required force to meet that condition for a range of target engine speeds.

From the results given in Table 4 and Figure 6-6 it is clear that the two requirements are at odds with each other. The first calls for the forces not to be excessively large to prevent a large energy dissipation rate per unit area of friction surface. The second requires the force to be large enough to guarantee that the shift can be completed. There are a few options to reconcile these requirements in the clutchless transmission. One is to assist the action of the synchronizer either with the electric motor or by the engine itself through the throttle, or both, so that the load is shared and the synchronizer bears a smaller load. Another way is to utilize slightly larger synchronizers such that the energy dissipation rate is smaller for larger forces. Lastly, an equal-sized synchronizer but with an extra friction ring can be used. This way the flank angle β_s can be designed smaller and the index torque will then be larger for a given force.

6.3 Other sources of failure

In addition to clashing and overheating, other sources of failure have been identified that are relevant for the clutchless transmission. One possible cause of failure is a slow displacement of the sleeve. After the two speeds have been synchronized and the ring unlocks, that is at the end of phase 4, there is no friction torque anymore to prevent one side to accelerate with respect to the other. Consequently, the difference in drag between the two sides may cause one side to accelerate faster than the other if the sleeve is not meshed fast enough [7]. High oil viscosity at low temperature may cause cold clash [22]. Cold clash may occur if the chamfer angle of the sleeve and ring teeth β is too small or the oil viscosity is too high at cold temperatures, in which cases blocking safety is not met. Excessive vibration may also be problematic. According to [23], increased wear on the friction surfaces may arise due to high vibrations in the transmission mechanism. Another possible source of failure is design of a wear gap that is too small. The wear

gap is a gap in the design of the ring that ensures that the ring continues to work even after it has worn some. If this gap is too small, the lifespan of the ring will be short [7]. Lastly, as mentioned before, if the cone angle is too small, self-locking may result between the blocker ring and the gear cone.

6.4 Case study

As an example of how to utilize the findings in this thesis, the following case studies are considered. The first one is for an upshift from 1st to 2nd gear starting with the engine at $9000rpm$ and the second one for a downshift between the same gears but starting with the engine at $2000rpm$.

For the upshift, assuming an initial engine speed mismatch of $100rpm$ and a shift force of $2000N$, Figure 5-5 says that the synchronization time would be under $10ms$. However, there is a minimum required force for any given target engine speed according to Figure 6-6. In this case, the target speed is the initial speed times the new ratio divided by the old ratio, or $9000rpm \cdot 2.185/3.077 \approx 6391rpm$. Then, from Figure 6-6 the minimum force is about $3.3kN$ which would make the synchronization time even lower. Extrapolating from Table 4, this should produce a specific power dissipation of about $1.5W/mm^2$.

For the downshift, assuming the same $100rpm$ of initial engine speed mismatch and $2000N$ force, Figure 5-6 says that the synchronization time should be under $50ms$. But again, the minimum force required force from Figure 6-6 must be considered. In this case the target gear is 1st and therefore the target speed is $2000rpm \cdot 3.077/2.185 \approx 2800rpm$. For that target speed, Figure 6-6 says that the minimum force is about $2800N$, which would again make the synchronization time faster but produce a specific power dissipation of about $1.3W/mm^2$ (extrapolating from Table 4).

In both cases, the resulting specific power dissipation is somewhat high compared to the $0.45W/mm^2$ found in literature for a manual transmission. This is a consequence of high engine drag and does not depend on the initial engine speed mismatch because, as shown in Figure 6-6, for a given target engine speed there is a minimum required force just to overcome the drag in phase 4 after the synchronization is done. To address this, either a more powerful synchronizer would be required or there should be some torque input from the electric motor or the engine itself to help overcome engine drag.

7 CONCLUSION

The objective of this work was to characterize the performance of synchronizers for their implementation on a hybrid, clutchless transmission. It is imperative to understand the potential and limitations of these devices because the removal of the clutch from the transmission induces increases the load they are normally subject to. After an overview of the process of synchronization was given, a simple mathematical model was presented building on prior art to represent the most important properties of the physical system. An experiment was designed to verify the model's validity and the experimental results were compared to the modeled results. Predictions were made for the behavior of the synchronizers under several different hypothetical configurations in the clutchless transmission. Possible failure modes were investigated for the most critical mechanical components so as to prevent complications in the new design.

7.1 Model validation

Given the many uncertainties that exist at the current stage of the clutchless transmission design, a model was needed that would correctly capture the behavior of synchronizers under the modified configuration without requiring all the details of every element. The presented model describes the behavior of the synchronizer unit with a minimum number of parameters. Seven parameters describe the synchronizer: the number of cones, the mean cone diameter, the cone angle, the coefficient of friction (assumed constant), the sleeve diameter, the sleeve flank angle, and the coefficient of friction of the sleeve teeth. The engine is described by two parameters: the rotational inertia and the drag torque reflected on the target gear. And the car as a whole is described by an equivalent rotational inertia and an equivalent rotational drag reflected on the output shaft of the transmission. The model was validated with an experiment setup that utilized a manual lathe to emulate the most important features of the vehicle transmission. In addition, the experiment demonstrated a simple way to indirectly estimate the rotational drag and inertia of a complex mechanism such as is the vehicle engine. With this, a simulator was created in Matlab to predict performance under any given configuration and for any desired constraints.

7.2 Predictions for clutchless transmission

The results provided important insights about the function of the synchronizer in the new transmission design. It was shown that due to the large engine inertia, the synchronization during an upshift can effectively be done with little fork force because the drag slows the engine down rapidly. On the other hand, during a downshift the engine drag must be overcome, so in this case a large fork force is required unless the process is assisted by an electric motor or by the engine itself through the throttle. Moreover, for a given target engine speed, there is a force threshold below which the synchronization will not succeed no matter how small the speed difference is. The reason is that the drag is stronger than the torques produced by forces below the threshold and so the speed difference would actually increase with time. This detrimental effect of the engine drag during a downshift is amplified for higher engine speeds. Increasing the mean diameter of the friction cones was shown to have a positive effect on performance. Increasing the number of cones has an even better outcome. But the mechanism becomes increasingly complex with each added intermediate cone. So when larger torque is needed, it must be achieved by balancing the increase of mean cone diameter and the addition of intermediate cones.

An important result that surfaced was that the requirement that the index torque be higher than the drag torque reflected on the gear implies that the forces on the selection fork must be high, in the order of $2kN$ to $3kN$. However, forces in this range produce a high energy dissipation rate per unit area of friction surface as compared with values in literature. Therefore it is recommended to either introduce more powerful synchronizers (with larger mean cone diameter or with an extra friction cone) or ensure that the synchronization is assisted by an external torque such as an electric motor to overcome the engine drag. In the first case, a high force would not produce such a large specific energy dissipation rate, and in the second case the high force would not be needed.

In general, this analysis has shown that although the magnitude of the speed difference to be synchronized largely affects the synchronization time, it does not significantly affect the likelihood of a successful shift. Whether or not a synchronization event can succeed is highly dependent on the balance between the torque produced by the fork force and the effective drag torque of the engine reflected on the gear. Nevertheless, further work is necessary to investigate how the duration of the synchronization affects the synchromesh performance.

7.3 Modes of failure

Failure mechanisms were investigated in contemplation of the more extreme conditions in which the synchronizers are expected to operate. An FEA analysis was performed on the blocker ring to identify the internal stresses that arise in the material due to the applied sleeve forces. The material ultimate tensile strength was measured with a Rockwell hardness testing machine and its yield stress was estimated from that value. Using those parameters it was found that for the geometry and material of the blocker ring described in section 5.1.2 the axial force that would cause it to permanently deform is approximately $17.8kN$. Compared to the nominal $1.5kN$ at which the same synchronizer normally operates, that force is about one order of magnitude larger, suggesting that, from a material strength perspective, the ring should withstand forces considerably larger than the nominal value without deforming or breaking. High wear of the friction surfaces appears to be the most common cause of failure according to literature. One important cause of rapid wear, other than misuse and impurities in the lubricant, is overheating of the friction rings. An energy analysis was performed to calculate the rate of energy dissipation per unit area of friction surface which was then compared to literature values. The specific energy dissipation rate (which was shown to be proportional to the applied fork force) calculated from the simulations was higher that found in literature for manual transmissions for forces above $1kN$. However, a manual transmission is expected to have a larger safety factor and thus it is estimated that forces between $1kN$ and $2kN$ are still within healthy limits in that respect. Other less common failure modes were mentioned for reference.

7.4 Future work

This work has focused primarily on one phase of the synchronization process where the actual speed synchronization happens. Future work is needed to investigate the other phases to guarantee that all the details are taken into account for designing synchronizers in the clutchless transmission. In particular, the requirement for full engagement in phase 4 that index torque must

be greater than drag torque was taken from literature but was not tested for the new configuration which is expected to have much larger inertia and drag. Likewise, the effect of the spring force from the detent was neglected in simulations based on previous research but not from experiment. Further experiments should be designed to address these concerns. In addition, integrated experiments should be carried out not only to validate the assumptions made here but also to measure effects such as wear, temperature, and vibration that were not tested in this work. Finally, the FEA analysis performed tested the strength of the material to withstand the possible applied loads but it did not test the effect of fatigue in the metal. If larger forces do end up being necessary, the effect of material fatigue should be tested in further experiments.

REFERENCES

[1] Robert Fischer, Ferit Küçükay, Gunter Jürgens, and Rolf Najork, *The Automotive Transmission Book*. Springer International Publishing Switzerland, 2015.

[2] J. Jurewicz, G. Pamanes, Y.S. Jo, P.X.T. Yen, J.E. Siegel, C.L. Jacoby, D. Dorsch, and A.G. Winter V, "Design Of A Clutch-Less Hybrid Transmission For A High-Performance Vehicle," *ASME IDETC CIE*, vol. ASME 2015 Power Transmission and Gearing Conference, no. 23rd Reliability, Stress Analysis, and Failure Prevention Conference. Paper #DETC2015–46812, Aug. 2015.

[3] Chih-Hsien Yu, Chyuan-Yow Tseng, and Chin-Ping Wang, "Smooth gear-change control for EV Clutchless Automatic Manual Transmission," *2012 IEEEASME Int. Conf. Adv. Intell. Mechatron.*, Jul. 2012.

[4] A. P. Bedmar, "Synchronization processes and synchronizer mechanisms in manual transmissions," Master's Thesis, Chalmers University of Technology, Göteborg, Sweden 2013, 2013.

[5] Umesh Wazir, "Manual Gearbox Synchronizers - An Overview," *Int. J. Emerg. Trends Eng. Dev.*, vol. 5, no. 3, 2013.

[6] Daniel Häggström, Pär Nyman, Ulf Sellgren, and Stefan Björklund, "Predicting friction in synchronizer systems," *Tribol. Int.*, vol. 97, pp. 89–96, 2016.

[7] Ottmar Back, "Basics of Synchronizers," *HOERBIGER Antriebstechnik GmbH*, 2013.

[8] Paul D. Walker and Nong Zhang, "Engagement and control of synchroniser mechanisms in dual clutch transmissions," *Elsevier*, vol. Mechanical Systems and Signal Processing, no. 26, pp. 320–332, 2012.

[9] Schaeffler KG, "Intermediate Rings for Multi-Cone Synchronizer Systems," *INA*, vol. Automotive Product Information API, no. 06, 2007.

[10] Chyuan-Yow Tseng and Chih-Hsien Yu, "Advanced shifting control of synchronizer mechanisms for clutchless automatic manual transmission in an electric vehicle," *Elsevier*, vol. Mechanism and Machine Theory, no. 84, pp. 37–56, 2015.

[11] H. Olsson, K.J. Åström, C. Canudas de Wit, and M. Gäfvert, "Friction Models and Friction Compensation," *Eur. J. Control*, no. 4, pp. 176–195, 1998.

[12] Xu Wanli, Zhao Wei, Su Bin, and Xu Ximeng, "Investigation of manual transmission synchronizer failure mechanism induced by interface material/lubricant combinations," *Elsevier BV*, vol. Wear, no. 328–329, pp. 475–479, 2015.

[13] Shibashis Ghosh, "Typical Coefficient of Friction Values for Common Materials," *MechGuru*, 2015-2008. .

[14] EngineersHandbook.com, "Coefficient of Friction," *Engineer's Handbook*, 2006. .

[15] Buff Furman, "Inertia Calculations," *ME 106 Fundamentals of Mechatronics*. .

[16] EngineeringToolBox.com, "Rolling Resistance," *The Engineering Tool Box*. .

[17] EngineeringToolBox.com, "Drag Coefficient," *The Engineering Tool Box*. .

[18] Mohammed Kamil, M.M. Rahman, and Rosli A. Bakar, "An integrated model for predicting engine friction losses in internal combustion engines," *Int. J. Automot. Mech. Eng.*, vol. 9, pp. 1695–1708, 2014.

[19] Ottmar Back, Peter Echtler, and Michael Bergheim, "Potential of Sintered Friction Linings in Synchronizers," *HOERBIGER Antriebstechnik GmbH*.

[20] R. C. Hibbeler, *Mechanics of Materials*, 9th ed. United States of America: Pearson Prentice Hall, 2014.

[21] John Fenton, Ed., "Transmission Gearboxes and Drive Line," in *Handbook of Automotive Design Analysis*, 1976, pp. 1–32.
[22] A. Sandooja and R. Kunai, "Automotive Synchronizer with Asymetric Toothing." [Online]. Available: http://papers.sae.org/2011-01-0724/. [Accessed: 30-Apr-2016].
[23] P. D. Walker and N. Zhang, "Transmission of Engine Harmonics to Synchronizer Mechanisms in Dual Clutch Transmissions," *J. Vib. Acoust.*, vol. 136, no. 5, pp. 051009–051009, Aug. 2014.

APPENDICES

Appendix A Simulator and optimizer for parameter determination

Instructions: Copy the following three functions and save them in files with names `optimization.m`, `sumSquares.m`, and `diff_e_spdl_for_optimization.m` respectively. Save the experimental data to a 4-column matrix in Matlab like `[time force angle omega]` and save the workspace as a .mat file e.g. `'data0307_24.mat'`. Run simulation by executing `optimization.m` .

```
% begin optimization.m
file_name = 'data0307_24.mat';
x0 = [0.1, 0.15, 0.5]; % [J, drag, f_coul] initial guess
[x, fval] = fminsearch(@(x) sumSquares(x,file_name,false),x0);
fprintf('\nJ = %f kg*m^2\nDrag coef = %f kg*m^2/s\nCoulomb torque = %f
N*m\n',x)
%% verify that the result is good
close all
sumSquares(x, file_name, true)
% end optimization.m

% begin sumSquares.m
function s = sumSquares(x,file_name,PLOT)
    % This function  takes in a force vector like simul_spdl.m does
    % and returns a value which is the sum of the squares of the errors
    % as compared to the experimental data
    J = x(1);
    drag = x(2);
    f_coul = x(3);
    load(file_name);
    vel_factor = 0.3429; % ratio of diameter of sensor to that of spindle
    tspan = data(:,1)-data(1,1);
    vel = data(:,4)*vel_factor; % velocity vector converted [rad/s]
    % Initial condition
    u_init = vel(1); % [rad/s]
    [t,u]=ode45(@(t,u)
diff_e_spdl_for_optimization(t,u,J,drag,f_coul,file_name), tspan, u_init);
    s = norm(u(:,1)-interp1(tspan, data(:,4)*vel_factor, t));
    if PLOT,
        plot(t,u(:,1),'o');
        title('Angular Velocity');
        xlabel('Time [s]');
        ylabel('\omega [rad/s]');

        hold on
        plot(tspan,data(:,4)*vel_factor)
        legend('Simulated','Experimental')
        pause(0.0001)
    end
end
% end sumSquares.m

% begin diff_e_spdl_for_optimization.m
function de=diff_e_spdl_for_optimization(t,u,J,drag,f_coul,file_name)
    load(file_name); % load experimental vector of forces
```

```
    time_data = data(:,1) - data(1,1);
    force_data = data(:,2);
    % ------------------------------------------------------
    dia_spdl = 0.16002; % [m] spindle diameter
    % ------------------------------------------------------
    % Force [N]
    force = interp1(time_data, force_data, t); % [N] shift force at sleeve
    % ------------------------------------------------------
    % Torque [N*m]
    f_torque = force*dia_spdl/2;
    % ------------------------------------------------------
    % Differential equation
    de = 1/J*(f_torque - drag*u(1) - f_coul);
end
% end diff_e_spdl_for_optimization.m
```

Appendix B Simulator for lathe experiments

Instructions: Copy the following three functions and save them in files with names `simul_spdl.m`, `diff_e_spdl.m`, and `events_spdl.m` respectively. Save the experimental data to a 4-column matrix in Matlab like `[time force angle omega]` and save the workspace as a .mat file e.g. `'data0307_20.mat'`. Run simulation by executing `simul_spdl.m` .

```
% begin simul_spdl.m
file_name = 'data0307_20.mat';
% load experimental data [time force angle omega]
load(file_name);
vel_factor = 0.3429; % ratio of diameter of sensor to that of spindle
tspan = data(:,1)-data(1,1);
vel = data(:,4)*vel_factor; % velocity vector converted [rad/s]
dia_spdl = 0.16002; %0.16002 [m] spindle diameter
torque = data(:,2)*dia_spdl/2;
% Initial condition
u_init = vel(1); % [rad/s]
options=odeset('Events',@events_spdl,'Stats','off'); %Create an options
variable
[t,u]=ode45(@(t,u) diff_e_spdl(t,u,file_name), tspan, u_init, options);
t_final = t(end);
%% Plot input torque and response with subplots
figure(1)
subplot(10,1,[1 3])
plot(tspan,torque,'r')
title('Input')
xlabel('Time [s]')
ylabel('Torque [N\cdotm]')
set(gca,'FontSize', 10,'FontWeight', 'normal', 'FontName', 'Times New Roman')
box off
subplot(10,1,[6 9])
plot(tspan,vel,'b')
title('Response')
xlabel('Time [s]')
ylabel('Speed [rad/s]')
set(gca,'FontSize', 10,'FontWeight', 'normal', 'FontName', 'Times New Roman')
box off
%% Plot experimental vs simulated
```

```
figure(2)
plot(tspan,vel,'bo')
hold on
plot(t,u,'r');
set(gca,'FontSize', 10,'FontWeight', 'normal', 'FontName', 'Times New Roman')
% title('Time response')%,'FontWeight','normal')
xlabel('Time [s]')
ylabel('\omega [rad/s]')
legend('Experimental', 'Simulated')
box off
% end simul_spdl.m

% begin diff_e_spdl.m
function de=diff_e_spdl(t,u,file_name)
load(file_name); % load experimental data [time force angle omega]
time_data = data(:,1) - data(1,1);
force_data = data(:,2);
% ------------------------------------------------------
dia_spdl = 0.16002; % [m] spindle diameter
J = 0.0427; % [kg*m^2] moment of inertia
drag = 0.026; % [kg*m^2/s] drag coefficient
f_coul = 0.177; % [N*m] Coulombic torque
% ------------------------------------------------------
% Force [N]
force = interp1(time_data, force_data, t); % [N] shift force at sleeve
% ------------------------------------------------------
% Torque [N*m]
f_torque = force*dia_spdl/2;
% ------------------------------------------------------
% Differential equation
de = 1/J*(f_torque - drag*u - f_coul);
end
% end diff_e_spdl.m

% begin events_spdl.m
function [value,isterminal,direction]=events_spdl(t,u)
        value=u; %Stops when angular velocity is zero
        isterminal=1; %Stop after the first event (=0 to get all the events)
        direction=0; % No matter which direction (+ -> -  or - -> +)
end
% end events_spdl.m
```

Appendix C Simulator for vehicle synchronization

Instructions: Copy the following three functions and save them in files with names `simul_veh.m`, `diff_e_veh.m`, and `events_veh.m` respectively. Run simulation by `simul_veh(shiftFrom, shiftTo, rpm_init, delta, F, mu, dia_cone, N_c, PLOT)`.

```
% begin simul_veh.m
function t_final = simul_veh(shiftFrom, shiftTo, rpm_init, delta,...
    F, mu, dia_cone, N_c, PLOT)
    % inputs: (shiftFrom='number of gear to shift from', shiftTo='number of
    %   target gear', rpm_init='starting rpm of engine', delta='starting
    %   engine speed difference', F='fork force in N', mu='cone cof',
    %   dia_cone='cone diameter in mm', N_c='number of cones', PLOT='true
```

```
    %   or false whether to plot or not')
    % output: synchronization time
    % [-] gear ratios for gears 1 to 7 (from F142_R02.xls)
    ratio = [3.077 2.185 1.626 1.286 1.028 0.839 0.69];
    wh0 = (rpm_init*pi/30)/ratio(shiftFrom); % [rad/s] initial speed of hub
    if shiftTo > shiftFrom, dir = 1; else dir = -1; end
    wg0 = wh0 + dir*(delta*pi/30)/ratio(shiftTo); % [rad/s] init speed gear
    % Initial conditions u = [gear_speed, hub_speed]
    u_init = [wg0 wh0]; % [rad/s]
    t0 = 0; % starting time
    tf = 0.51; % time limit
    dt = 1e-3; % time step
    options = odeset('Events',@events_veh,'Stats','off'); % options variable
    [t,u] = ode45(@(t, u) diff_e_veh(t, u, dir, F, ratio(shiftTo), ...
      mu,dia_cone,N_c), t0:dt:tf, u_init, options);
    t_final = t(end);
    %%plot
    if PLOT,
        plot(t*1e3,u(:,1),'--b',t*1e3,u(:,2),'-.r');
        xlabel('Time [ms]');
        ylabel('Angular velocity [rad/s]');
        legend('Engine side of synchro.','Wheels side of synchro.')
    end
end
% end simul_veh.m

% begin diff_e_veh.m
function de=diff_e_veh(t,u,dir,F,r_et,mu,dia_cone,N)
% input: (t='time vector', u=[speed_gear, speed_hub], dir='direction of
%   shift (1 or -1)', F='fork force in N', r_et='ratio of engine to target
%   gear', mu='cone cof', dia_cone='cone diameter in mm', N='number of
%   cones')
% output: differential equation o u
% ------------------------------------------------------------------
% Parameters
N_c = N; % [-] default 3 number of cones
Mu_c = mu; % [-] default 0.1 COF of cones
R_c = dia_cone/2/1000; % [m] default 84.1/2/1000 mean cone radius
alpha_c = 6.55*pi/180; % [rad] cone angle
Mu_s = 0.12; % [-] COF of sleeve and fork
R_s = 112.17/2/1000; % [m] mean sleeve radius
% ------------------------------------------------------------------
% Fork force
F_f = F; % [N] default 1500
% ------------------------------------------------------------------
% Inertia [kg*m^2]
Jg = 0.1052*r_et^2; % engine reflected inertia on gear
Jh = 7.2028; % car reflected inertia on hub
% ------------------------------------------------------------------
% Friction torque [N*m]
Ts = dir*(N_c*Mu_c*R_c*F_f)/(sin(alpha_c)); % synchronization torque
Tf = Mu_s*F_f*R_s; % the friction between sleeve and fork
% ------------------------------------------------------------------
% Drag torque [N*m]
Tdg = 0.1526*r_et*u(1) + 35.0141*r_et; % engine reflected drag torque on gear
Tdh = 0.000137*u(2)^2 + 0.01045*u(2) + 9.5982; % car torque on hub
% ------------------------------------------------------------------
% Differential equations [1/s^2]
```

```
gear_de = 1/Jg*(-Ts - Tdg); % differential equation of gear side
hub_de = 1/Jh*(Ts - Tdh - Tf); % differential equation of hub side
de = [gear_de; hub_de];
end
% end diff_e_veh.m

% begin events_veh.m
function [value,isterminal,direction]=events_veh(t,u)
    value=u(1)-u(2); %Stops when angular velocity difference is zero
    isterminal=1; %Stop after the first event (=0 to get all the events)
    direction=0; % No matter which direction (+ -> -  or - -> +)
end
% end events_veh.m
```